Electronic Supplementary Material (ESI) for Chemical Communications.

Supporting Information

for

Enhancing barrier height for Yb(III) single-ion magnets by modulating axial ligand fields

Aditya Borah, Sourav Dey, Sandeep K. Gupta, Mrinalini G. Walawalkar, Gopalan Rajaraman* and Ramaswamy Murugavel*

Department of Chemistry, Indian Institute of Technology Bombay, Mumbai-400076, India

Experimental Section

Instruments and Methods: All the reactions were performed at ambient reaction conditions. Fourier-transform infrared spectra were recorded on a Perkin Elmer Spectrum One spectrometer using KBr diluted pellets. The ESI-MS studies were carried out on Bruker MaXis impact mass spectrometer. Microanalyses were performed on a Thermo Finnigan (FLASH EA 1112) microanalyzer. Powder X-ray diffractions were recorded on a Philips X'pert Pro (PANalytical) diffractometer using Cu Kα radiation (λ = 1.54190 Å). The magnetic properties of the polycrystalline samples were measured using a Quantum Design MPMS-XL SQUID magnetometer equipped with a 7 T magnet in the temperature range 2-300 K. The magnetic properties of **1–3** were measured on phase pure polycrystalline powder samples. The data were corrected for the background diamagnetic contribution and the diamagnetic contribution of the compounds were corrected using Pascal's constants. Alternating current (ac) susceptibility measurements were performed with an oscillating ac field of 3.5 Oe oscillating at indicated frequencies between 0.1 and 1500 Hz. The solid state X-band EPR measurements were made on Bruker spectrometers, at IIT Bombay, with a helium gas-flow cryostat. The X-band measurements were carried out at 5K.

Materials: Commercial grade solvents were purified by employing conventional procedures[1]. $YbX_3.xH_2O$ were prepared from Yb_2O_3 (Alfa Aesar) by digesting in the respective acid, (HX = HNO_3 (**1**), TfOH (**2**) and HI (**3**) followed by drying under vacuum. Triphenylphosphine oxide (Sigma Aldrich) was used as received. The hydroiodic acid (laboratory grade, containing traces of HBr/HCl) was used as received to prepare $YbX_3.xH_2O$.

Synthesis and characterisation of **$[Yb(Ph_3PO)_4(NO_3)_2][NO_3]\cdot C_2H_5OH$ (1)** ***and*** **$[Yb(Ph_3PO)_4(OTf)_2][OTf]\cdot(C_2H_5OH)_{0.5}$ (2)**

To a hot ethanolic solution (20 mL) of $YbX_3.xH_2O$ (X= NO_3 (**1**) and OTf (**2**)) (0.25 mmol) was added a ethanolic solution of Ph_3PO (347 mg, 1.25 mmol) under reflux condition. The reaction mixture was heated under reflux for 4 h and cooled down to room temperature. The solution was then filtered and the filtrate was kept for crystallization at room temperature. Colourless block shaped crystals were obtained within 24 hours. The product has been washed 2-3 times with cold ethanol.

$[Yb(Ph_3PO)_4(NO_3)_2][NO_3]\cdot C_2H_5OH$ (1): Yield: 0.310 g (84.2%, based on ligand), FT-IR (KBr, cm^{-1}): 3423 (s), 3057 (s), 1618 (w), 1590 (w), 1484 (s), 1437 (s), 1384 (s), 1298 (s), 1186 (w), 1155 (vs), 1121 (s), 1092 (m), 1030 (w), 997 (w), 928 (w), 815 (w), 747 (m), 724 (vs), 693 (s), 541 (vs). ESI-MS: 1410.2789; $[M\text{-}NO_3]^-$. Elemental analysis (in %) found (Calculated) for $C_{74}H_{66}N_3O_{14}P_4Yb_1$: C, 58.60 (58.54); H, 4.033 (4.38); N 2.67 (2.77).

$[Yb(Ph_3PO)_4(OTf)_2][OTf]\cdot(C_2H_5OH)_{0.5}$ (2): Yield: 0.335 g (77%, based on ligand), FT-IR (KBr, cm^{-1}): 3232 (b), 3063 (s), 1613 (w), 1590 (m), 1486 (m), 1438 (vs), 1333 (s), 1278 (m), 1207 (m), 1136 (vs), 1122 (vs), 1081 (s), 1030 (s), 998 (w), 928 (w), 850 (w), 748 (m), 726 (vs), 693

(s), 636 (vs), 542 (vs), 519 (w). ESI-MS : 1584.2034; $[M-OTf]^{-}$**.** Elemental analysis (in %) found (Calculated) for $C_{76}H_{63}F_9O_{13.5}P_4S_3Yb_1$: C, 52.35 (51.97); H, 3.50 (3.62); S 5.53 (5.48).

***Synthesis and characterisation of* 3**

To a hot ethanolic solution (20 mL) of $YbI_3.xH_2O$ (0.25 mmol) was added a ethanolic solution (10 mL) of Ph_3PO (347 mg, 1.25 mmol) under reflux condition. Yellow precipitate was formed within 10 minutes, the reaction is allowed to reflux for 1 hour. 30 mL Dichloromethane has been added to the reaction mixture and heated under reflux for 2 hours for complete dissolution of the product. The light red solution was then filtered and the filtrate was kept for crystallization at room temperature. Dark brown block shaped crystals were obtained within 1-2 weeks. The crystals have been washed two times with cold ethanol. With the help of crystallography studies, the product was identified as $Yb(Ph_3PO)_4(I_{0.53}Br_{0.47})(I_{0.38}Cl_{0.62})][I_3]\cdot C_2H_5OH$ rather than the expected $[Yb(Ph_3PO)_4(I)_2]I_3$. The presence of chloride and bromide impurities in the molecule was further confirmed by ESI Mass studies producing additional peaks at m/z 1448 for $[Yb(Ph_3PO)_4(I)(Cl)][I_3]$ and at m/z 1357 for $[Yb(Ph_3PO)_4(Cl)_2][I_3]$. (Figure S2b).

$Yb(Ph_3PO)_4(I_{0.53}Br_{0.47})(I_{0.38}Cl_{0.62})][I_3]\cdot C_2H_5OH$ (3): FT-IR (KBr, cm^{-1}): Yield: 0.28 g (67%, based on ligand), 3173 (b), 3053 (s), 1589 (m), 1484 (m), 1437 (s), 1313 (w), 1280 (w), 1186 (w), 1144 (vs), 1121 (vs), 1086 (s), 1026 (w), 997 (w), 928 (w), 851 (w), 746 (m), 724 (vs), 691 (s), 542 (vs). ESI-MS: m/z= 1540 for $[Yb(Ph_3PO)_4(I)_2]^+$, 1448 for $[Yb(Ph_3PO)_4(I)(Cl)]^+$ and 1357 for $[Yb(Ph_3PO)_4(Cl)_2]^+$**.** Elemental analysis for single crystals (in %) found (Calculated) for $C_{74}H_{66}Br_{0.47}Cl_{0.62}I_{3.91}O_5P_4Yb_1$: C, 45.49 (46.93); H, 3.23 (3.28). The elemental analysis of bulk, polycrystalline sample, showed minor variations from the calculated values due to varying amounts of chloride and bromide impurities in place of axial iodide ligands (see Fig. S33b-c)

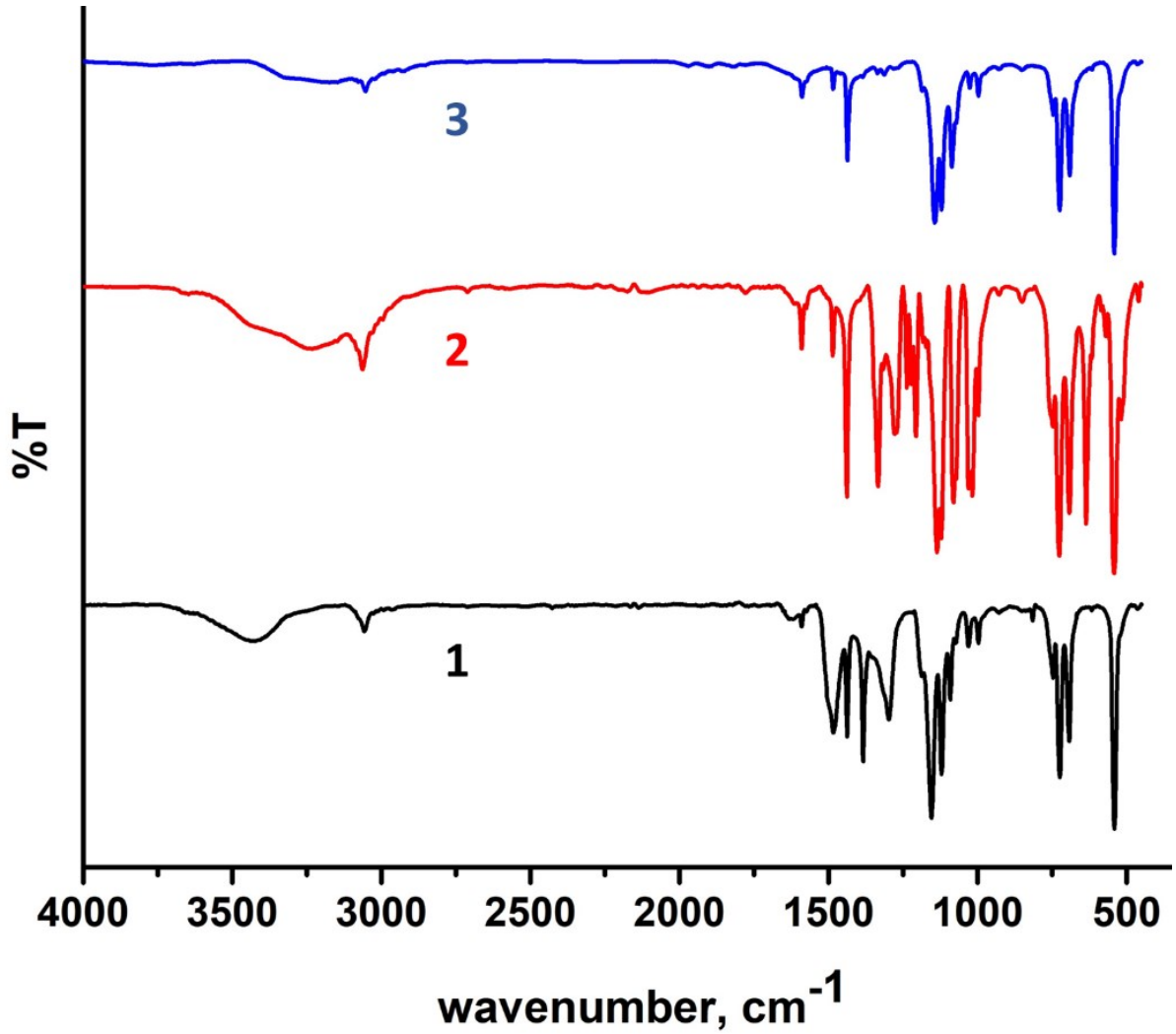

Figure S1. FTIR spectra of the complexes **1-3** as disc diluted with KBr.

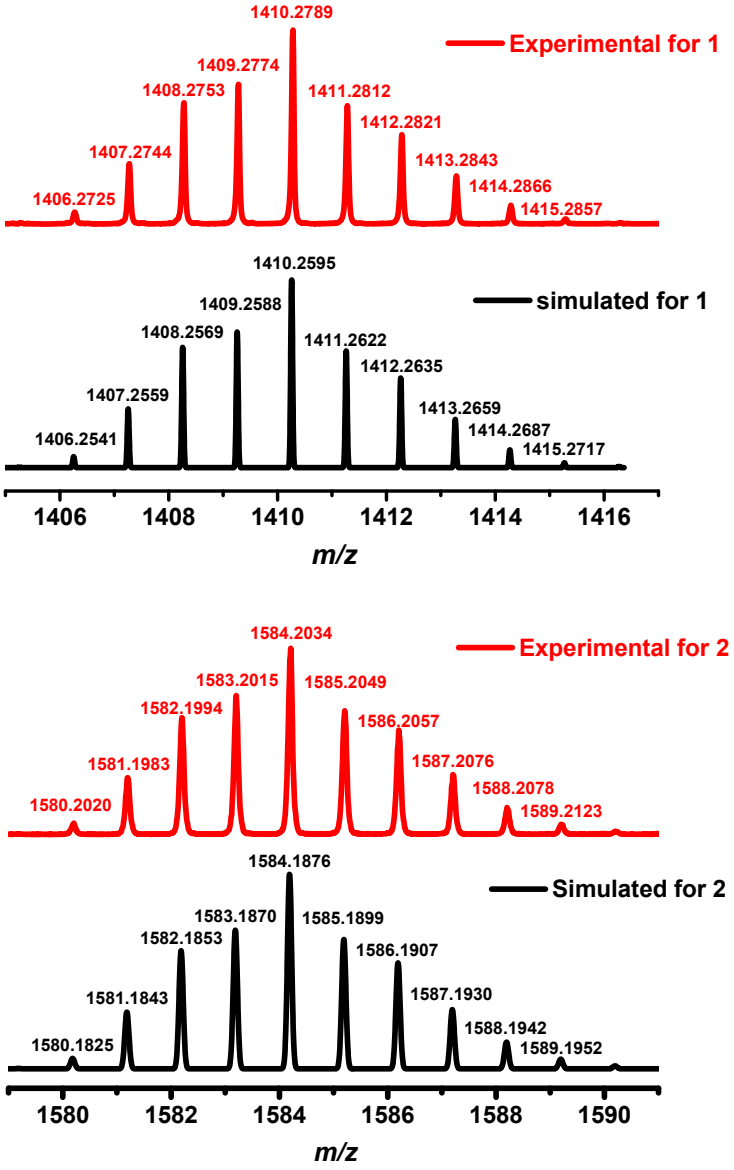

Figure S2a. Molecular ion peaks in the ESI-MS spectrum of **1**, and **2** in methanol

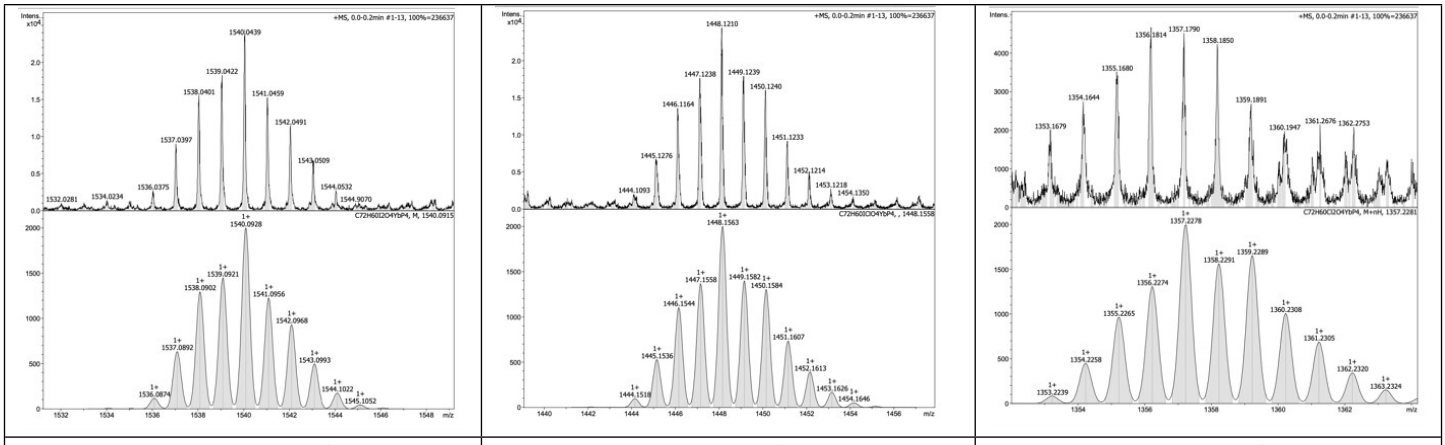

Figure S2b. ESI-MS of single crystalline **3** in acetonitrile solution, showing molecular ion peaks the three species indicated above, confirming the presence of other halo-impurities along with iodide.

Single Crystal X-ray Crystallography

Suitable blocked shaped single crystals of **1**-**3** were selected and mounted on a Rigaku Saturn 724+ CCD diffractometer at 150K using Paratone oil for unit cell determination and three dimensional intensity data collection. Data integration and indexing was carried out using CrysAlisPro. The crystal was kept at 150 K during data collection. Using Olex2[2], the structure was solved with the ShelXT[3] structure solution program using Intrinsic Phasing and refined with the ShelXL[4] refinement package using Least Squares minimisation.

Table-S1. Crystal data and structure refinement details for **1**-**3**.

Identification code	**1 (Yb_1)**	**2(Yb_2)**	**3 (Yb_3)**
CCDC number	1985219	1985220	1985221
Empirical formula	$C_{74}H_{66}N_3O_{14}P_4Yb_1$	$C_{152}H_{126}F_{18}O_{27}P_8S_6Yb_2$	$C_{74}H_{66}Br_{0.47}Cl_{0.62}I_{3.91}O_5P_4Yb_1$
Molecular formula	$[Yb(Ph_3PO)_4(NO_3)_2][NO_3]\cdot C_2H_5OH$	$[Yb(Ph_3PO)_4(OTf)_2][OTf]\cdot(C_2H_5OH)_{0.5}$	$Yb(Ph_3PO)_4(I_{0.53}Br_{0.47})(I_{0.38}Cl_{0.62})][I_3]\cdot C_2H_5OH$
Formula weight	1518.21	3512.72	1884.24
Temperature/K	150(2)	100(2)	123(2)
Crystal system	orthorhombic	triclinic	triclinic
Space group	Pccn	P-1	P-1
a/Å	15.9815(4)	13.6979(2)	13.9941(2)
b/Å	16.5996(3)	14.6330(2)	15.4903(3)
c/Å	26.6002(6)	19.8834(2)	17.7810(4)
α/°	-	94.599(1)	89.738(2)
β/°	-	108.159(1)	84.044(2)
γ/°	-	90.614(1)	80.588(1)
Volume/Å^3	7056.7(3)	3772.1(1)	3781.7(1)
Z	4	1	2
ρ_{calc}g/cm^3	1.429	1.546	1.655
μ/mm^{-1}	1.482	1.493	3.231
F(000)	3092	1772	1822
Crystal size/mm^3	0.088 × 0.06 × 0.04	0.15 × 0.06 × 0.03	0.12 x 0.075 x 0.07
Radiation / Å	MoKα (λ = 0.71073)	MoKα (λ = 0.71073)	MoKα (λ = 0.71073)
Theta range for data collection	2.340 to 24.996°.	2.492 to 24.998°	2.519 to 26.000°
Index ranges	-19<=h<=13 -19<=k<=19 -31<=l<=31	-16<=h<=16 -17<=k<=17 -23<=l<=23	-17<=h<=17 -19<=k<=19 -21<=l<=21
Reflections collected	32667	143550	121805
Independent reflections	6204 [R(int) = 0.0550]	13224 [R(int) = 0.0496]	14849 [R(int) = 0.0949]
Refinement method	Full-matrix least squares on F^2	Full-matrix least-squares on F^2	Full-matrix least-squares on F^2
Data/restraints/parameters	6204 / 22 / 461	13224 / 73 / 1024	14849 / 211 / 852
Goodness-of-fit on F^2	1.076	1.087	1.078
Final R indexes [I>=2σ (I)]	R1 = 0.0377, wR2 = 0.0936	R1 = 0.0375, wR2 = 0.0933	R1 = 0.0606, wR2 = 0.1284
Final R indexes [all data]	R1 = 0.0486, wR2 = 0.1008	R1 = 0.0394, wR2 = 0.0955	R1 = 0.0833, wR2 = 0.1404
Largest diff. peak/hole /eÅ^{-3}	1.301 / -0.746	1.182/ -1.009	1.219/ -0.493

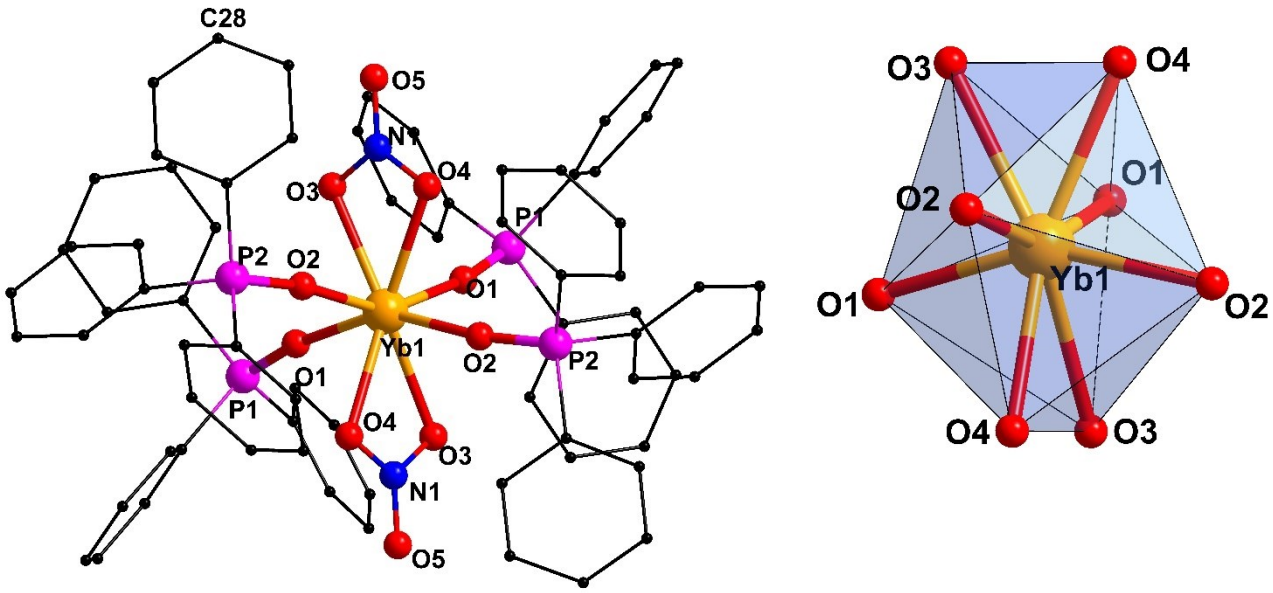

Figure S3(A) : (Left) Molecular structure of **1.** Hydrogen atoms, lattice nitrate anion and lattice ethanol molecules are omitted for clarity. (Right) Coordination environment of Yb(III) ion in **1**.

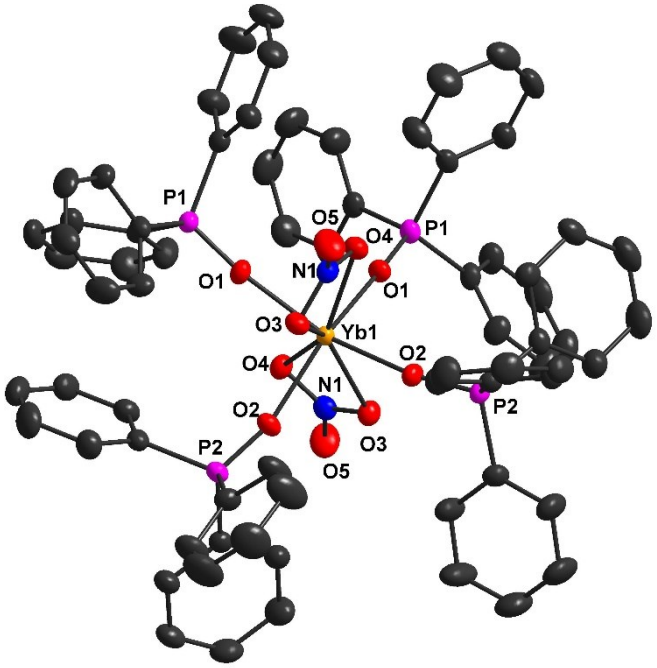

Figure S3(B) : ORTEP plot of the cationic part of **1** representing thermal ellipsoid with 50% probability. Hydrogen atoms, lattice nitrate anion and lattice ethanol molecules are omitted for clarity.

Table S2: Selected bond lengths (Å) and bond angles (°) in **1**

Yb(1)-O(1)#1	2.213(3)	O(1)#1-Yb(1)-O(1)	89.50(15)
Yb(1)-O(1)	2.213(3)	O(2)-Yb(1)-O(3)#1	75.39(9)
Yb(1)-O(2)	2.245(3)	O(2)#1-Yb(1)-O(3)#1	77.66(10)
Yb(1)-O(2)#1	2.245(3)	O(1)#1-Yb(1)-O(3)	130.37(9)
Yb(1)-O(3)#1	2.407(3)	O(1)-Yb(1)-O(3)	79.93(10)
Yb(1)-O(3)	2.407(3)	O(2)-Yb(1)-O(3)	77.67(10)
Yb(1)-O(4)	2.439(3)	O(2)#1-Yb(1)-O(3)	75.39(9)
Yb(1)-O(4)#1	2.439(3)	O(3)#1-Yb(1)-O(3)	141.12(13)
O(1)#1-Yb(1)-O(2)	95.37(10)	O(1)#1-Yb(1)-O(4)	77.54(9)
O(1)-Yb(1)-O(2)	154.23(10)	O(1)-Yb(1)-O(4)	79.23(10)
O(1)#1-Yb(1)-O(2)#1	154.23(10)	O(2)#1-Yb(1)-O(4)	128.23(10)
O(1)-Yb(1)-O(2)#1	95.37(10)	O(2)-Yb(1)-O(4)	77.18(10)
O(2)-Yb(1)-O(2)#1	91.16(14)	O(3)#1-Yb(1)-O(4)	142.38(9)
O(1)#1-Yb(1)-O(3)#1	79.93(10)	O(3)-Yb(1)-O(4)	52.89(9)
O(1)-Yb(1)-O(3)#1	130.36(9)	O(1)#1-Yb(1)-O(4)#1	79.23(10)
O(1)-Yb(1)-O(4)#1	77.54(9)	O(2)#1-Yb(1)-O(4)#1	77.18(10)
O(2)-Yb(1)-O(4)#1	128.22(10)	O(4)-Yb(1)-O(4)#1	147.07(13)
O(3)#1-Yb(1)-O(4)#1	52.89(9)	O(3)-Yb(1)-O(4)#1	142.38(9)

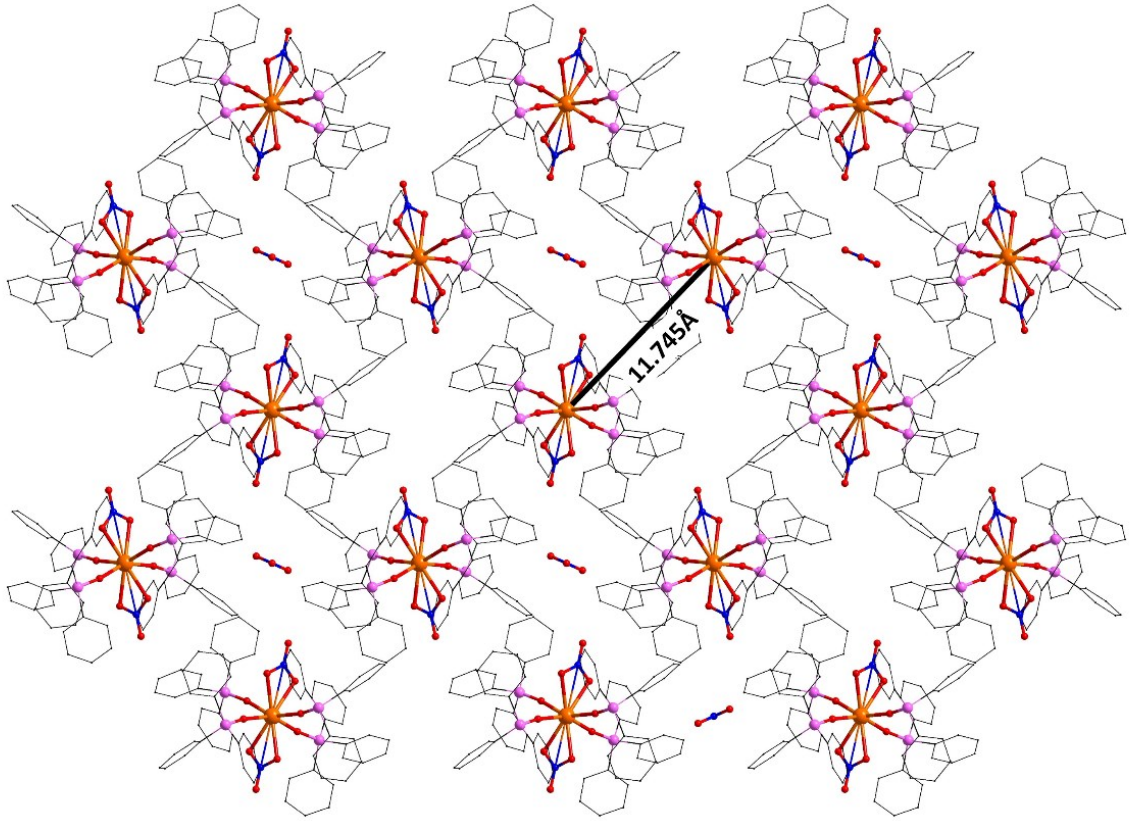

Figure S4: Lattice arrangement in the crystal of **1**. The bulky aryl groups and the presence of nitrate anion in the lattice leads the Yb(III) centres placed away from each other at a distance of 11.745 Å. Hydrogen atoms are omitted for clarity.

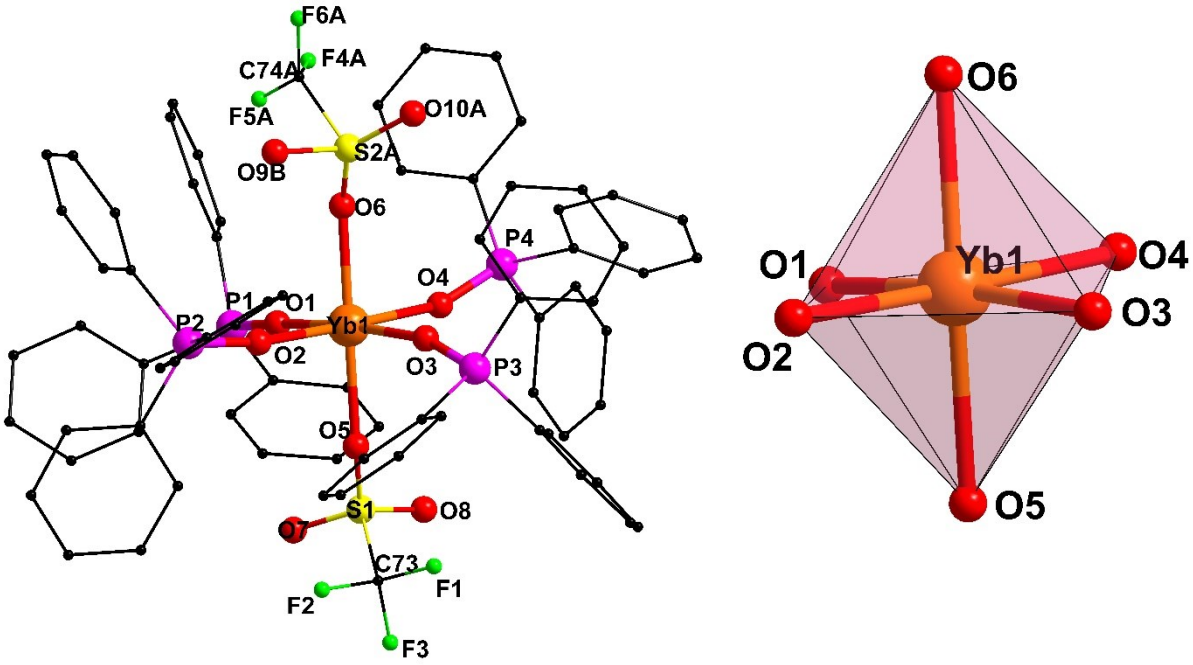

Figure-S5(A): (Left) Molecular structure of **2**, Only one part of the disordered coordinated triflate anion is shown for clarity. Hydrogen atoms, lattice triflate anion and lattice ethanol molecules are omitted for clarity. (Right) Coordination environment of Yb(III) ion in **2**.

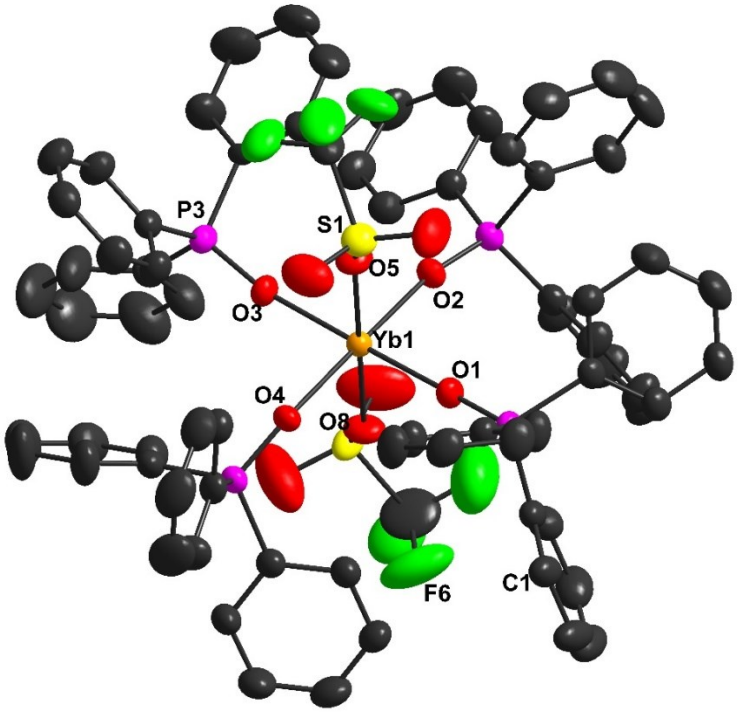

Figure-S5(B) : ORTEP plot of cationic part of **2** representing thermal ellipsoid with 50% probability. Only one part of the disordered coordinated triflate anion is shown for clarity. Hydrogen atoms, lattice triflate anion and lattice ethanol molecules are omitted for clarity.

Table S3: Selected bond lengths (Å) and bond angles (°) in **2**

Yb(1)-O(2)	2.172(2)	O(3)-Yb(1)-O(4)	89.32(9)
Yb(1)-O(3)	2.189(2)	O(1)-Yb(1)-O(4)	87.72(9)
Yb(1)-O(1)	2.198(2)	O(2)-Yb(1)-O(8)	92.41(10)
Yb(1)-O(4)	2.203(2)	O(3)-Yb(1)-O(8)	94.21(11)
Yb(1)-O(8)	2.224(3)	O(1)-Yb(1)-O(8)	91.75(11)
Yb(1)-O(5)	2.248(3)	O(4)-Yb(1)-O(8)	85.98(10)
O(2)-Yb(1)-O(3)	91.06(10)	O(2)-Yb(1)-O(5)	88.58(10)
O(2)-Yb(1)-O(1)	92.08(9)	O(3)-Yb(1)-O(5)	86.54(10)
O(3)-Yb(1)-O(1)	173.15(9)	O(1)-Yb(1)-O(5)	87.45(10)
O(2)-Yb(1)-O(4)	178.37(9)	O(4)-Yb(1)-O(5)	93.02(10)
O(8)-Yb(1)-O(5)	178.75(10)		

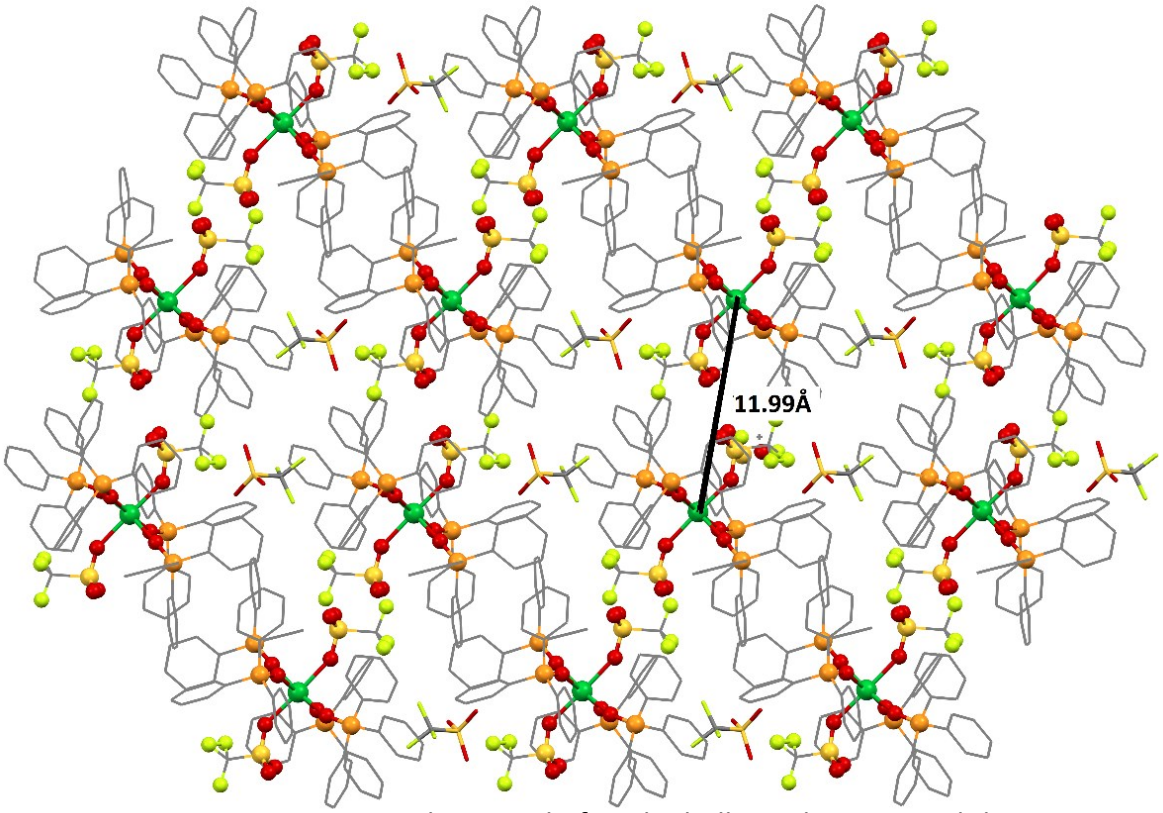

Figure S6: Lattice arrangement in the crystal of **2**. The bulky aryl groups and the presence of triflate anion in the lattice leads the Yb(III) centres placed away from each other at a distance of 11.99 Å. Hydrogen atoms are omitted for clarity.

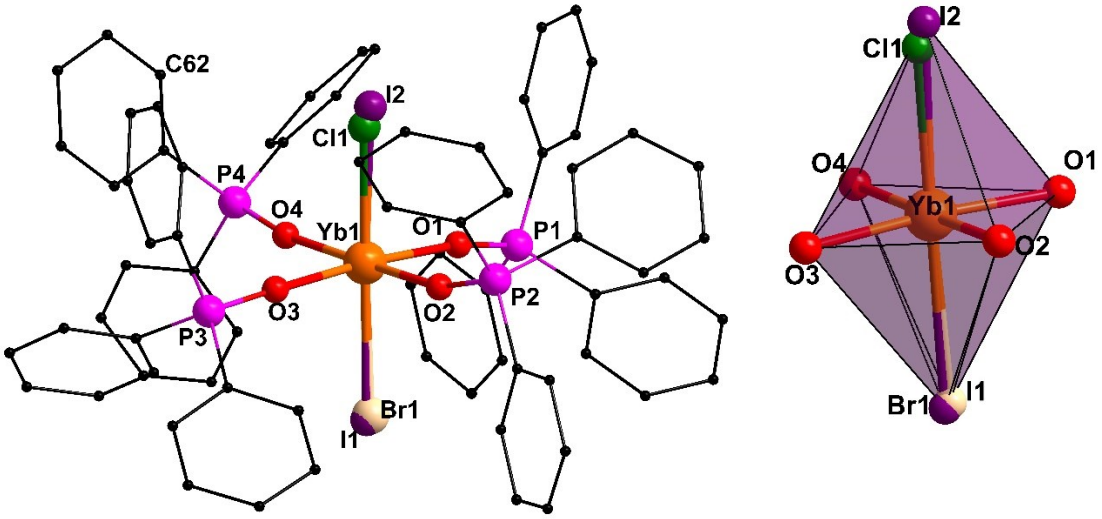

Figure S7(A): (Left) Molecular structure of **3,** Hydrogens and lattice anions are omitted for clarity. (Right) Coordination environment of Yb(III) ion in **3**. Hydrogen atoms and lattice triiodide anion are omitted for clarity.

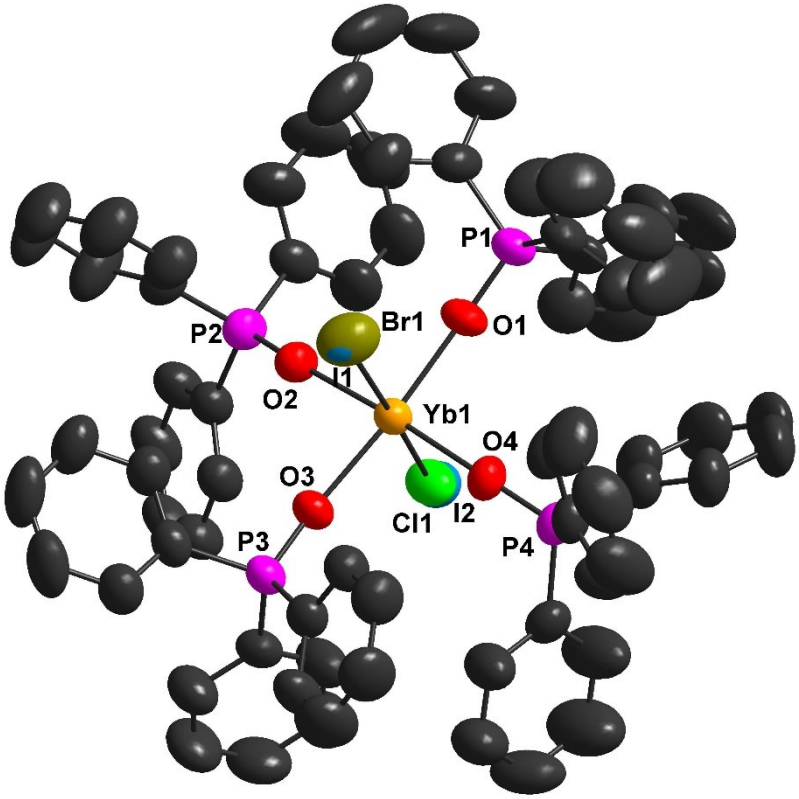

Figure-S7(B) : ORTEP plot of cationic part of **3** representing thermal ellipsoid with 50% probability. Hydrogen atoms and lattice triiodide anion are omitted for clarity.

Table S4: Selected bond lengths (Å) and bond angles (°) in **3**

Yb(1)-O(1)	2.169(4)	O(4)-Yb(1)-Cl(1)	88.6(5)
Yb(1)-O(4)	2.182(4)	O(2)-Yb(1)-Cl(1)	89.1(5)
Yb(1)-O(2)	2.187(4)	O(3)-Yb(1)-Cl(1)	91.5(4)
Yb(1)-O(3)	2.200(4)	O(1)-Yb(1)-Br(1)	87.5(2)
Yb(1)-Cl(1)	2.598(12)	O(4)-Yb(1)-Br(1)	93.1(2)
Yb(1)-Br(1)	2.899(9)	O(2)-Yb(1)-Br(1)	89.2(2)
Yb(1)-I(2)	2.970(6)	O(3)-Yb(1)-Br(1)	89.0(2)
Yb(1)-I(1)	2.973(4)	Cl(1)-Yb(1)-Br(1)	178.2(5)
P(1)-O(1)	1.504(4)	O(1)-Yb(1)-I(2)	89.5(2)
P(2)-O(2)	1.508(4)	O(4)-Yb(1)-I(2)	90.0(2)
P(3)-O(3)	1.493(4)	O(2)-Yb(1)-I(2)	87.8(2)
P(4)-O(4)	1.505(4)	O(3)-Yb(1)-I(2)	93.8(2)
O(1)-Yb(1)-O(4)	93.07(16)	Br(1)-Yb(1)-I(2)	175.8(3)
O(1)-Yb(1)-O(2)	90.13(16)	O(1)-Yb(1)-I(1)	89.27(15)
O(4)-Yb(1)-O(2)	176.12(15)	O(4)-Yb(1)-I(1)	92.56(14)
O(1)-Yb(1)-O(3)	175.14(15)	O(2)-Yb(1)-I(1)	89.68(13)
O(4)-Yb(1)-O(3)	90.51(15)	O(3)-Yb(1)-I(1)	87.29(14)
O(2)-Yb(1)-O(3)	86.43(15)	Cl(1)-Yb(1)-I(1)	178.3(5)
O(1)-Yb(1)-Cl(1)	91.9(4)	I(2)-Yb(1)-I(1)	177.19(19)

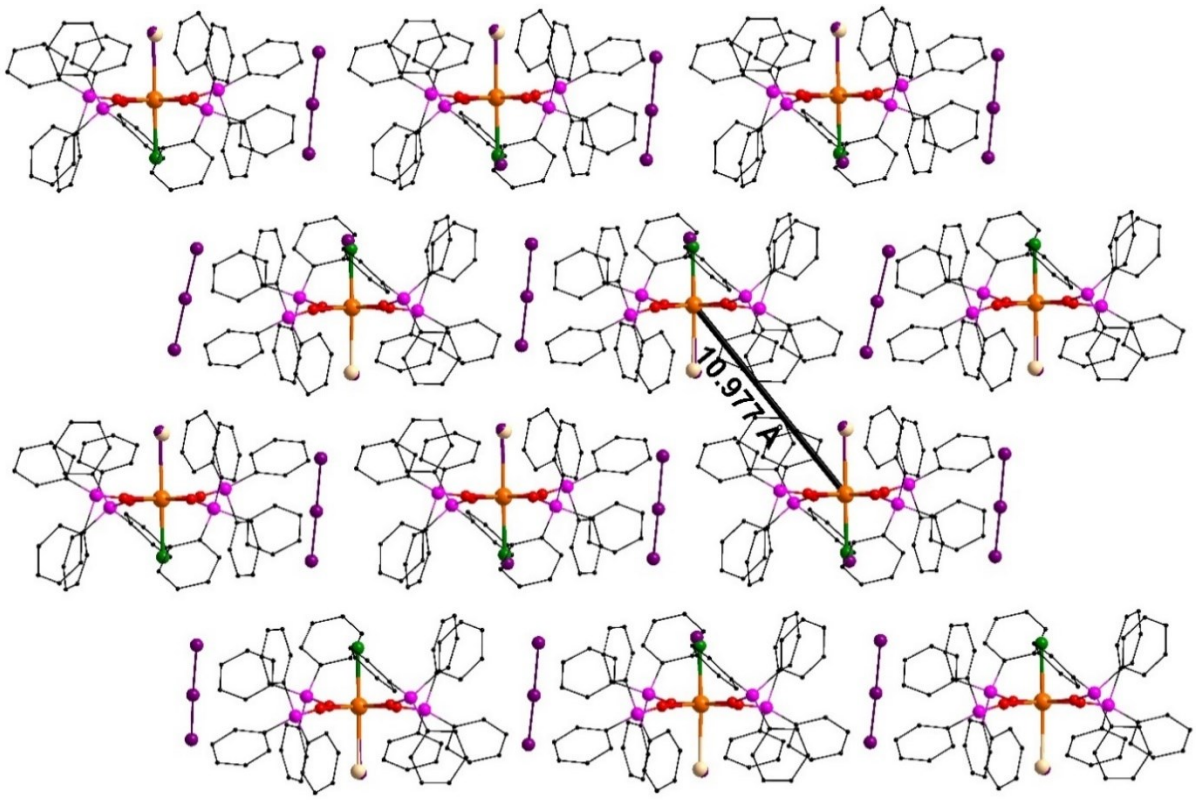

Figure S8: Lattice arrangement in the crystal of **3**. The bulky aryl groups and the presence of triiodide anion in the lattice leads the Yb(III) centres placed away from each other by a distance of 10.976 Å. H atoms are omitted for clarity.

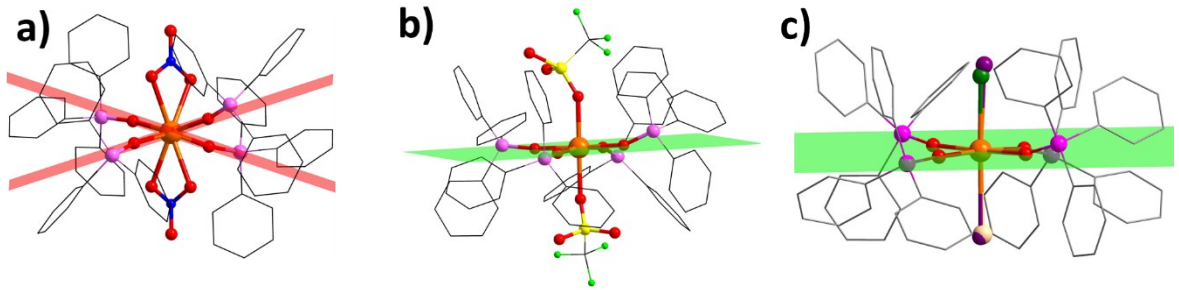

Figure **S9**: The coplanarity of the equatorial Ph_3PO ligands are represented for **1**-**3**. (a) The four O atoms of Ph_3PO ligands are not in the same plane due to the presence of two nitrate anions coordinated to Yb(III) centers via chelation in case of **1**. (b-c) The four oxygen atoms of Ph_3PO are coplanar along with Yb(III) in case of **2** and **3**. (Yb, orange; O, red; P, pink; N, blue; S, yellow; F, bright green; Cl, dark green; Br, tan; I, violet and C, black)

Table S5. Continuous Shape measures[5] of the coordination polyhedra of eight coordinated Yb(III) in **1.**

Label	**Symmetry**	**Shape**	**Deviation**
OP-8	D8h	Octagon	28.736
HPY-8	C7v	Heptagonal pyramid	24.723
HBPY-8	D6h	Hexagonal bipyramid	13.026
CU-8	Oh	Cube	11.881
SAPR-8	D4d	Square antiprism	4.759
TDD-8	***D2d***	***Triangular dodecahedron***	***2.791***
JGBF-8	D2d	Johnson gyrobifastigium J26	9.627
JETBPY-8	D3h	Johnson elongated triangular bipyramid J14	25.302
JBTPR-8	C2v	Biaugmented trigonal prism J50	3.752
BTPR-8	C2v	Biaugmented trigonal prism	3.531
JSD-8	***D2d***	***Snub diphenoid J84***	***2.326***
TT-8	Td	Triakis tetrahedron	12.709
ETBPY-8	D3h	Elongated trigonal bipyramid	22.898

Table S6. Continuous Shape measures of the coordination polyhedra of six-coordinated Yb(III) in **2** and **3.**

Label	Symmetry	Shape	Deviation in **2**	Deviation in **3I_2**	Deviation in **3IBr**	Deviation in **3ICl**	Deviation in **3ClBr**
HP-6	D6h	Hexagon	32.287	33.664	33.868	33.583	33.143
PPY-6	C5v	Pentagonal pyramid	27.972	28.283	28.083	28.573	28.346
OC-6	***Oh***	***Octahedron***	**0.146**	**2.325**	**2.185**	**1.591**	**1.405**
TPR-6	D3h	Trigonal prism	14.907	17.131	16.692	16.936	16.706
JPPY-6	C5v	Johnson pentagonal pyramid J2	31.558	30.936	30.739	31.275	31.080

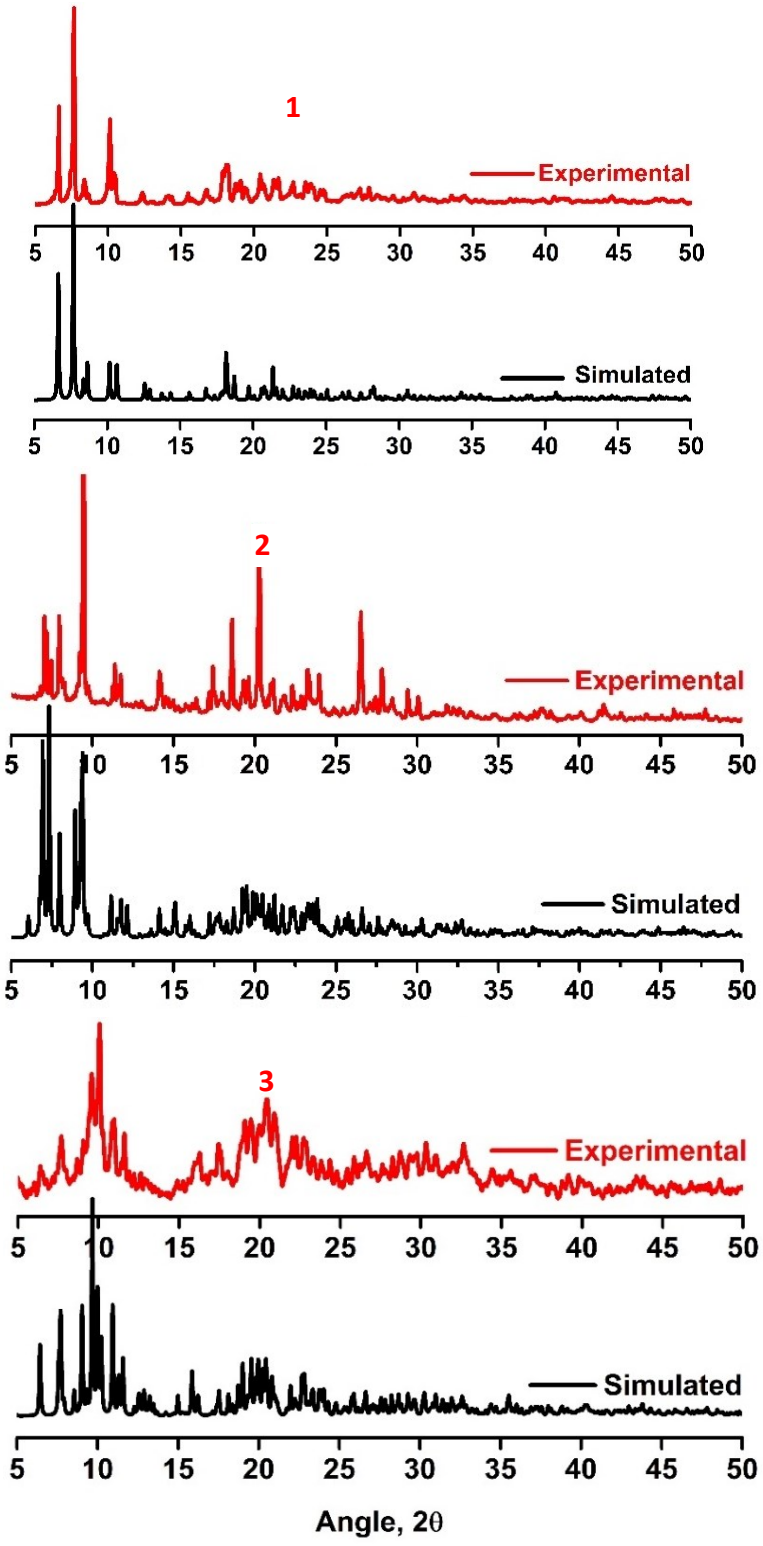

Figure S10.
Simulated

(black) and experimental (red) PXRD pattern of **1**-**3**.

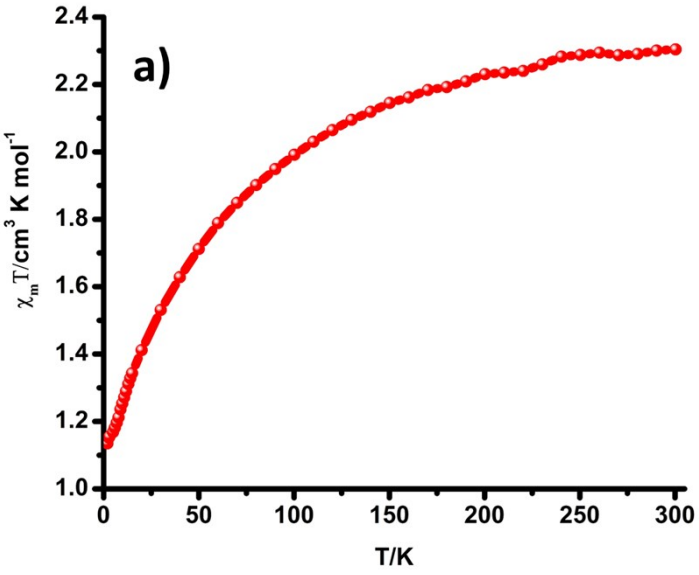

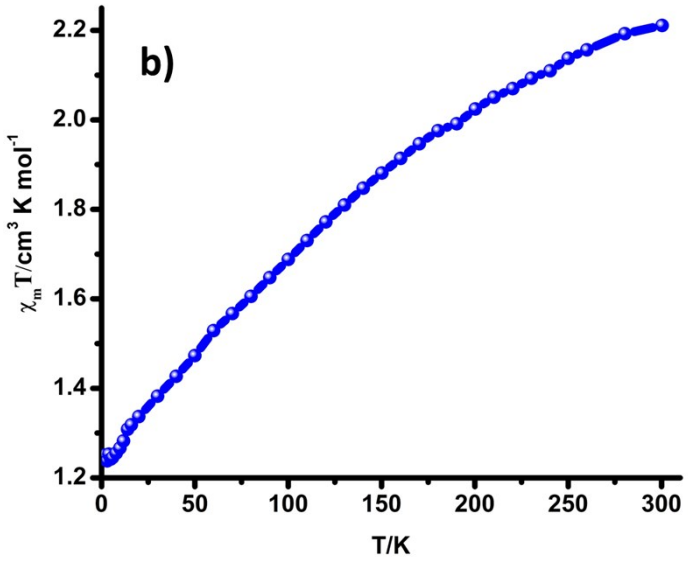

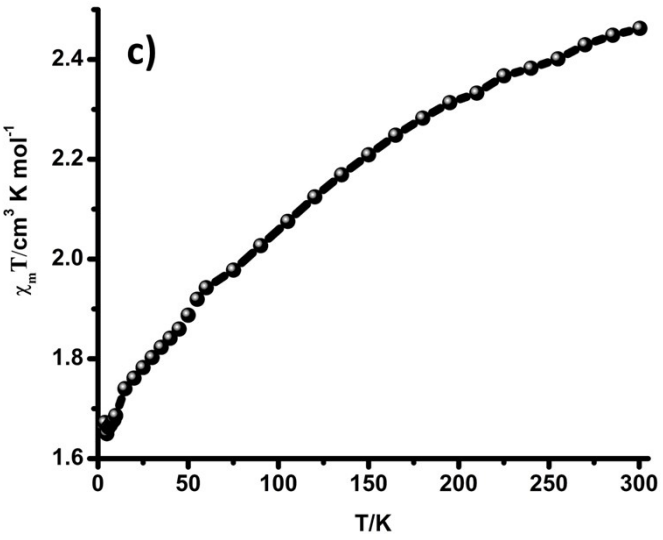

Figure S11. The temperature-dependence of magnetization data for **1** (a), **2** (b) and **3** (c) at different temperatures at 0.1T

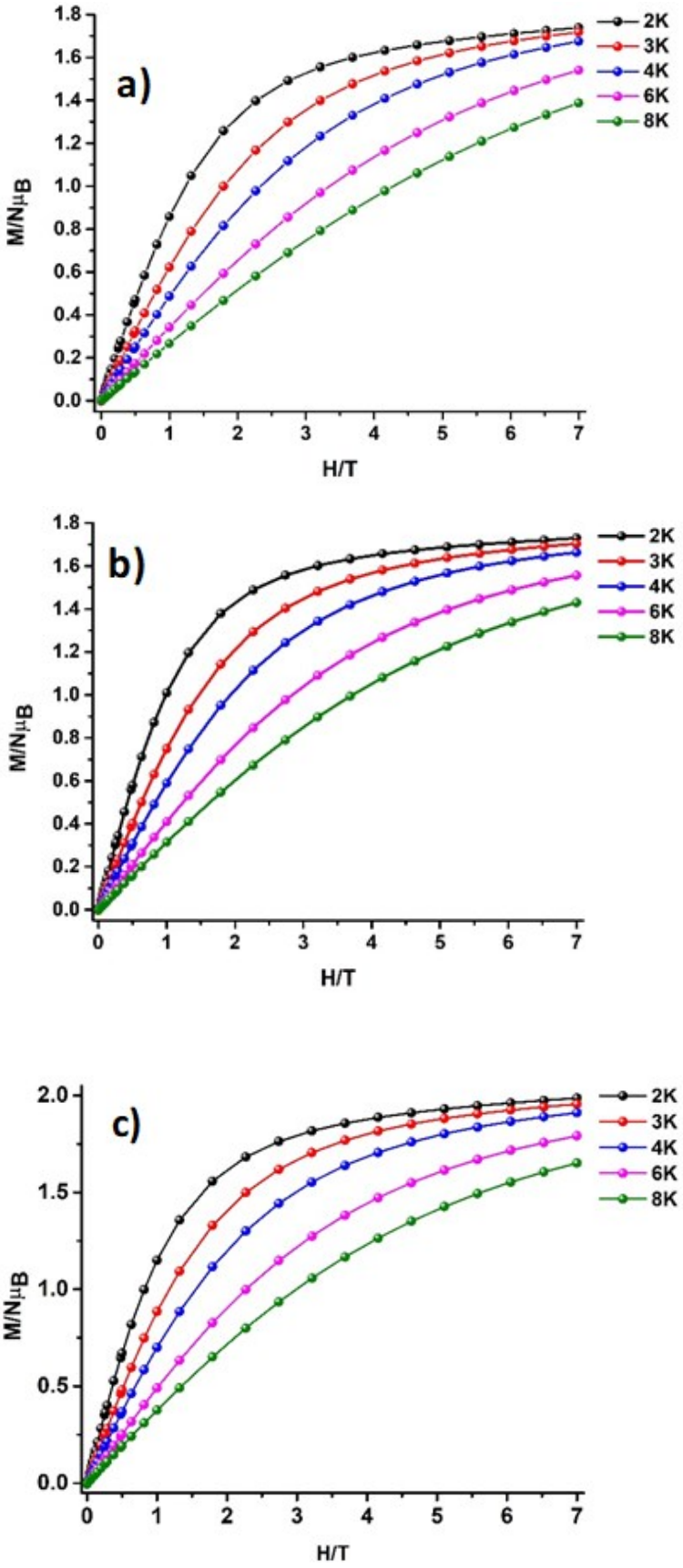

Figure S12. The field-dependence of magnetization data for **1** (a), **2** (b) and **3** (c) at different temperatures (2K, 4K, 6K and 8K).

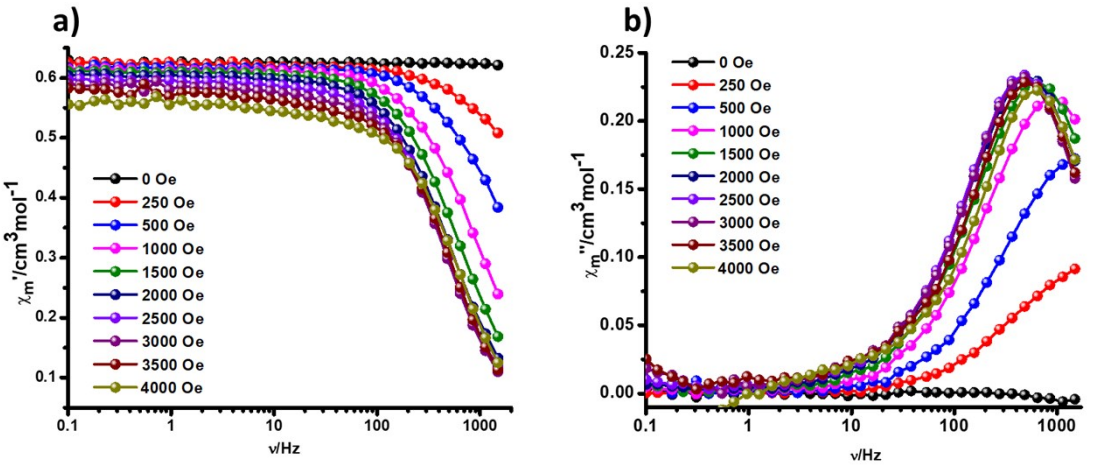

Figure S13: Frequency dependence of (a) in-phase (χ') and (b) out-of-phase (χ'') molar magnetic susceptibility for complex **1** in the presence of various dc fields at 1.8 K.

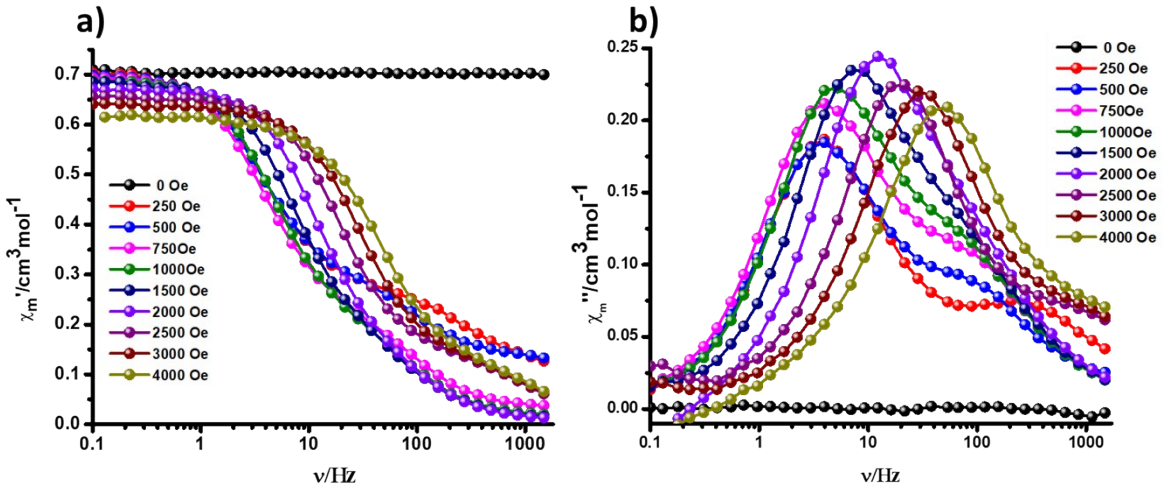

Fi

gure S14: Frequency dependence of (a) in-phase (χ') and (b) out-of-phase (χ'') molar magnetic susceptibility for complex **2** in the presence of various dc fields at 1.8 K

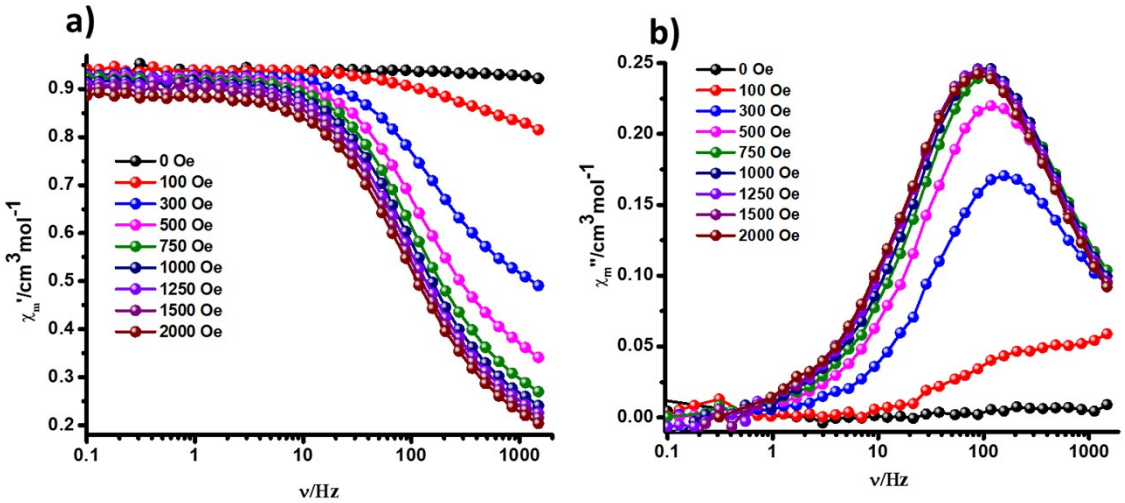

Figure S15: Frequency dependence of (a) in-phase (χ') and (b) out-of-phase (χ'') molar magnetic susceptibility for complex **3** in the presence of various dc fields at 1.8 K

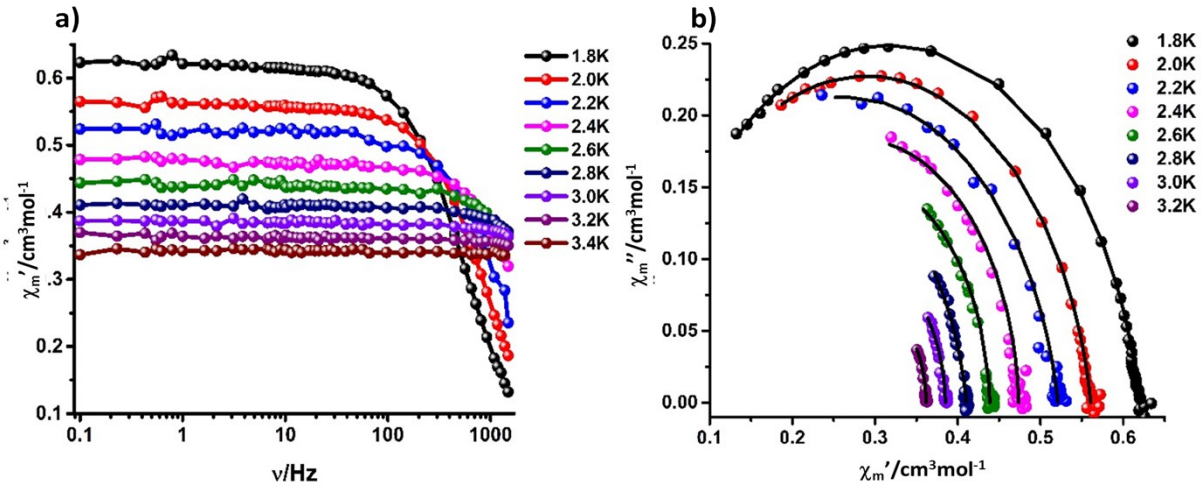

Figure S16: (a) Frequency dependence of in-phase molar magnetic susceptibility (χ') for complex **1** under an applied dc field of 2.5KOe. Solid lines are guides for the eyes. (b) Cole–Cole plot for **1** under an applied dc field of 2.5KOe. Solid black lines are the best fit to the Debye model.

The Cole-Cole data were fitted by considering single relaxation process using the generalized Debye model, as follows:

$$\chi_{AC}(\omega) = \chi_S + \frac{\chi_T - \chi_S}{1 + (i\omega\tau)^{(1-\alpha)}} \qquad \text{..... eq.1}$$

where χ_S =adiabatic susceptibility, χ_T = isothermal susceptibility, ω=angular frequency, τ = relaxation time, and α reflects the extent of distribution of the relaxation times.

Table-S7. Fitting parameters for Cole-Cole plot for complex **1**

T/K	χ_S	χ_T	τ	α	Residual
1.8	0.0189630	0.620083	0.284381E-03	0.119263	0.626371E-03
2.0	0.0184624	0.560877	0.181048E-03	0.111424	0.599484E-03
2.2	0.00857502	0.521165	0.114522E-03	0.117712	0.155168E-02
2.4	0.0900189	0.473562	0.873418E-04	0.0294192	0.185653E-02
2.6	0.106817	0.438657	0.576918E-04	0.0291069	0.431154E-03
2.8	0.129297E-13	0.410521	0.232696E-04	0.105359	0.294226E-03
3.0	0.184360	0.385030	0.346972E-04	0.0199938	0.172327E-03
3.2	0.222879	0.361623	0.313728E-04	0.00434066	0.947230E-04

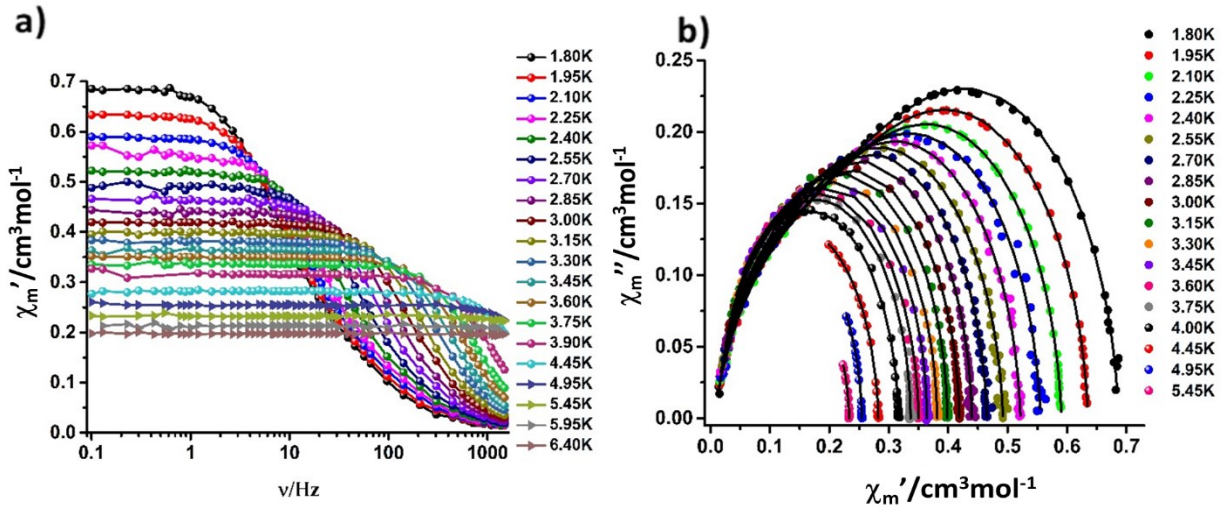

Figure 17 : (a) Frequency dependence of in-phase molar magnetic susceptibility (χ') for complex **2** under an applied dc field of 2KOe. Solid lines are guides for the eyes. (b) Cole–Cole plot for **2** under an applied dc field of 2KOe. Solid black lines are the best fit to the Debye model.

The Cole-Cole plot was fitted by considering two relaxation process using the modified Debye model, as follows

$$\chi_{AC}(\omega) = \chi_{S1} + \chi_{S2} + \frac{\chi_{T1} - \chi_{S1}}{1 + (i\omega\tau_1)^{(1-\alpha_1)}} + \frac{\chi_{T2} - \chi_{S2}}{1 + (i\omega\tau_2)^{(1-\alpha 2)}} \quad \text{.....eq.2}$$

Table-S8. Fitting parameters for Cole-Cole plot for complex **3**

T (K)	$\chi_{S,tot}$	$\Delta\chi_1$	τ_1	α_1	$\Delta\chi 2$	$\tau 2$	$\alpha 2$	Residual
1.8	0.692620E-02	0.285980E+00	0.305447E-02	0.199625E+00	0.394385E+00	0.259701E-01	0.433038E-01	0.659628E-03
1.95	0.536316E-02	0.280657E+00	0.263245E-02	0.219798E+00	0.349673E+00	0.197655E-01	0.328229E-01	0.195109E-03
2.1	0.574814E-02	0.260901E+00	0.208949E-02	0.218306E+00	0.324260E+00	0.139663E-01	0.237098E-01	0.154092E-03
2.25	0.707352E-02	0.198075E+00	0.129622E-02	0.179174E+00	0.350392E+00	0.920587E-02	0.413563E-01	0.139371E-02
2.4	0.441676E-02	0.197040E+00	0.107210E-02	0.193512E+00	0.320204E+00	0.612081E-02	0.280300E-01	0.509928E-03
2.55	0.666777E-02	0.122638E+00	0.568762E-03	0.132621E+00	0.362821E+00	0.364596E-02	0.509082E-01	0.753604E-03
2.7	0.805448E-02	0.114067E+00	0.458982E-03	0.114757E+00	0.342810E+00	0.246108E-02	0.384664E-01	0.408081E-03
2.85	0.114292E-01	0.810447E-01	0.294456E-03	0.151147E-01	0.347417E+00	0.164649E-02	0.321283E-01	0.619901E-03
3	0.120271E-01	0.767899E-01	0.252906E-03	0.334894E-03	0.329961E+00	0.114142E-02	0.324363E-01	0.198425E-03
3.2	0.980885E-02	0.604979E-01	0.176771E-03	0.545740E-02	0.328327E+00	0.781788E-03	0.257609E-01	0.286838E-03
3.3	0.857915E-02	0.585654E-01	0.149662E-03	0.980848E-02	0.314274E+00	0.568671E-03	0.297612E-01	0.140908E-03
3.45	0.637159E-02	0.651639E-01	0.125462E-03	0.123814E-01	0.292744E+00	0.427022E-03	0.166866E-01	0.298214E-03
3.60	0.217472E-06	0.377389E-01	0.600890E-04	0.533043E-01	0.312468E+00	0.294563E-03	0.311813E-01	0.880237E-04
3.75	0.796969E-03	0.401393E-01	0.521206E-04	0.251932E-01	0.295700E+00	0.230122E-03	0.189971E-01	0.157916E-03
4	0.588611E-02	0.139970E-01	0.301067E-04	0.351820E-01	0.296250E+00	0.145337E-03	0.266241E-01	0.781187E-04
4.45	0.165215E-02	0.183541E-14	0.162403E-04	0.774519E-03	0.280693E+00	0.671323E-04	0.304545E-01	0.687950E-04
4.95	0.203405E-01	0.119753E-14	0.925788E-05	0.226137E-02	0.234159E+00	0.398235E-04	0.126610E-01	0.425551E-04
5.45	0.162537E-01	0.249920E-01	0.340466E-05	0.111766E-01	0.192005E+00	0.256485E-04	0.393980E-01	0.125809E-03

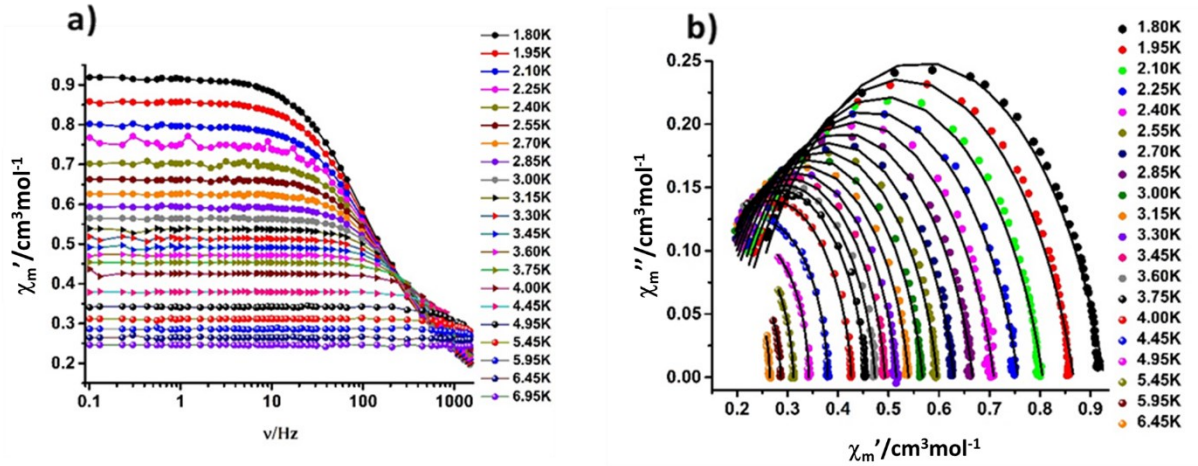

Figure S18: (a) Frequency dependence of in-phase molar magnetic susceptibility (χ') for complex **3** under an applied dc field of 1KOe. Solid lines are guides for the eyes. (b) Cole–Cole plot for **3** under an applied dc field of 1KOe. Solid black lines are the best fit to the Debye model. The data were fitted by considering single relaxation process using eq.1

Table-S9. Fitting parameters for Cole-Cole plot for complex **3**

T/K	χ_S	χ_T	τ	α	Residual
1.8	0.2018	0.92681	0.0014	0.23393	0.00274
1.95	0.186648	0.86655	0.0012	0.22893	0.00296
2.1	0.175129	0.80538	0.00102	0.22003	0.00232
2.25	0.165445	0.75678	8.86638E-4	0.21335	0.00184
2.4	0.158072	0.70864	7.60574E-4	0.19482	0.00246
2.55	0.150977	0.66658	6.44677E-4	0.18166	0.00159
2.7	0.145367	0.62947	5.46487E-4	0.16846	0.00138
2.85	0.139551	0.59633	4.67216E-4	0.15417	9.51012E-4
3	0.133227	0.56703	3.95457E-4	0.14526	8.39321E-4
3.15	0.128102	0.53959	3.34594E-4	0.13311	6.70898E-4
3.3	0.124888	0.51545	2.86664E-4	0.12173	5.59474E-4
3.45	0.121915	0.49295	2.44328E-4	0.10833	5.23124E-4
3.6	0.115679	0.47316	2.08335E-4	0.10544	3.65741E-4
3.75	0.113421	0.45431	1.79011E-4	0.09095	1.95887E-4
4	0.109848	0.42629	1.40366E-4	0.07899	1.30296E-4
4.45	0.119948	0.37949	9.5183E-5	0.03495	1.57871E-4
4.95	0.116776	0.34195	6.35832E-5	0.02161	1.1919E-4
5.45	0.0855024	0.31152	3.70296E-5	0.04508	6.38011E-5
5.95	0.111451	0.2861	3.03908E-5	0.02247	2.83403E-5
6.45	0.0947135	0.26447	2.1235E-5	0.00842	1.13128E-4

Table-S10: Comparison of magnetism of **1-3** with other reported mononuclear Yb(III)-based SIMs.

Sl no.	Complex	Coordination number	H(dc)/ Oe	U_{eff} /K	τ_0/s	Ref.
1	**1**	**8**	**2500**	**9.58**	**2.26×10^{-6}**	**This work**
2	**2**	**6**	**2000**	**28.16**	**2.88×10^{-8}**	**This work**
3	**3**	**6**	**1000**	**21.27**	**8.34×10^{-7}**	**This work**
4	$[Yb^{III}(H_3L)_2]Cl_3 \cdot 5CH_3OH \cdot 2H_2O$, H_3L = tris(((2-hydroxy-3-methoxybenzyl)amino)ethyl)-amine	6	400	6.86	2.0×10^{-5}	6
5	$[Yb(H_3Bmshp)(DMF)_2Cl_2] \cdot DMF \cdot 1.5H_2O$ $[Yb(H_3Bmshp)(DMF)_2Cl_2] \cdot H_4Bmshp$ (H_4Bmshp = (2,6-bis[(3-ethoxysalicylidene) hydrazinecarbonyl]-pyridine))	7 7	1500 600	14.5 38.3	2.38×10^{-5} 7.16×10^{-7}	7
6	Yb(trensal), H_3trensal=2,2′,2″-tris(salicylideneimino)triethylamine	7	2000	53.2	1.5×10^{-8}	8
7	$Yb(NO_3)_3(tBu_3PO)_2$	8	1000	23.0	6.8×10^{-7}	9
8	$[Yb(tta)_3(L)] \cdot 2CH_2Cl_2$	8	1500	6	1.9×10^{-5}	10
9	$[Yb(QR1)_2][NO_3](CH_3OH)(H_2O)_{0.5}$ $[Yb(QR1)(tta)_2](CH_3OH)$	8 8	1000 1000	5.37 16.1	$1.0x\ 10^{-5}$ 1.78×10^{-7}	11
10	$[Cp^*Yb(DAD)(THF)] \cdot C_7H_8$ enediamido[2,6-Me2C6H3NCH=CHNC$_6$H$_3$Me$_2$-2,6]$_2$– (DAD)	8	1500	19.6	1.74×10^{-6}	12
11	$[Yb(9\text{-}Accm)_2(NO_3)(dmf)_2]$	8	750	28.9	4.6×10^{-8}	13
13	$Na[YbDOTA(H_2O)] \cdot 4H_2O$	9	1000	29	4×10^{-7}	14
14	$[Yb(Tpz)_2Bpz] \cdot CH_2Cl_2$ Tpz = hydrotris(pyrazolyl)-borate Bpz = dihydrobis(pyrazolyl)borate)	9	1500	28	2×10^{-8}	15

Computational Details

Post Hatree-Fock *ab initio* CASSCF/RASSI-SO/SINGLE_ANISO calculation has been performed using MOLCAS 8.2 programme package[16]. The relativistic effect of Yb has been taken into account by DKH Hamiltonian[17]. The disk space of the two electron integral has been reduced by cholesky decomposition technique[18]. We have used ANO-RCC VTZP basis set for Yb; VDZP basis set for O, N, F,Cl,Br and I; VDZ basis set for P, C and H. All the basis sets have been taken from the ANO-RCC library implemented in MOLCAS 8.2 programme package. The CASSCF calculation has been performed with considering thirteen electrons in seven 4f orbitals i.e., using CAS (13,7) active space. We have computed seven doublet CSFs (configuration state functions) using this active space. These CSFs have been mixed by RASSI-SO to compute spin-orbit energy levels[19]. Finally, the g tensor, magnetic susceptibility, molar magnetisation, barrier height for magnetisation reversal have been calculated using the SINGLE_ANISO which interfaced with RASSI-SO energies[20].

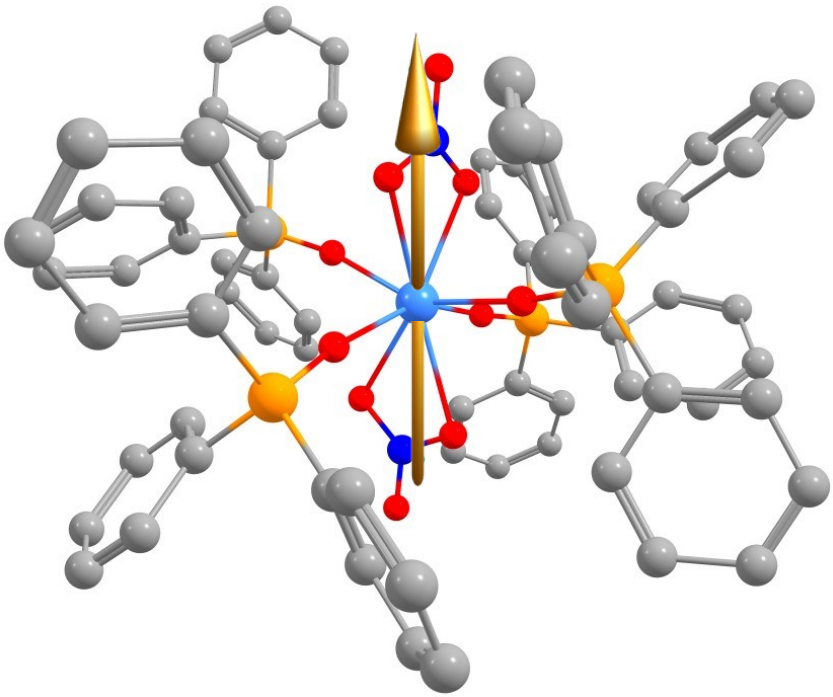

Figure S19: The g_{zz} anisotropy axis of complex **1**. Colour code: Yb-sky blue; O-red; N-blue; P-orange; C-grey. Hydrogens are omitted for clarity.

Table-S11. The energy of the four Kramers doublets along with g tensor of complex **1**.

Energy (cm^{-1})	g_x	g_y	g_z
0.0	0.939	1.264	7.007
90.5	0.434	2.581	4.966
225.5	0.964	1.072	7.235
290.5	0.504	1.150	7.297

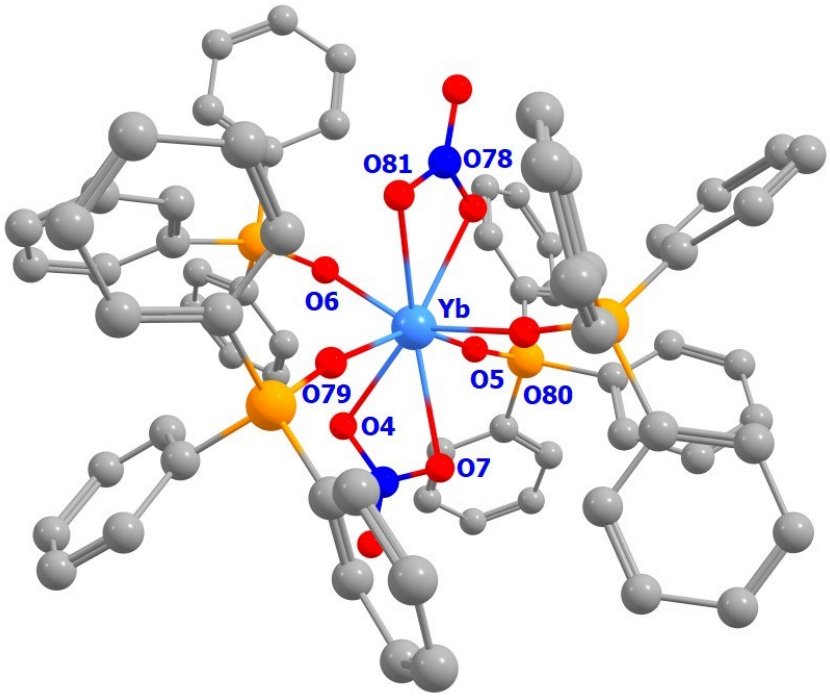

Figure S20: Model for Atom number with LoProp charge of **1**. Colour code: Yb-sky blue; O-red; N-blue; P-orange; S-green yellow; F-light yellow; C-grey. Hydrogens are omitted for clarity. The increase in the LoProp charge along the equatorial plane increases the axiality of this complex compared to **1** which is also reflected in the increase of the B_2^0 value (also see Fig. S23, S24 and Tables S12, S13, S19, S20).

Table-S12. LoProp charge of Yb and coordinated atoms with Yb of complex **1**.

Atom	LoProp charge
Yb	2.5523
O78	-0.6510
O81	-0.6426
O79	-1.0896
O80	-1.0854
O4	-0.6509
O5	-1.0894
O6	-1.0855
O7	-0.6426

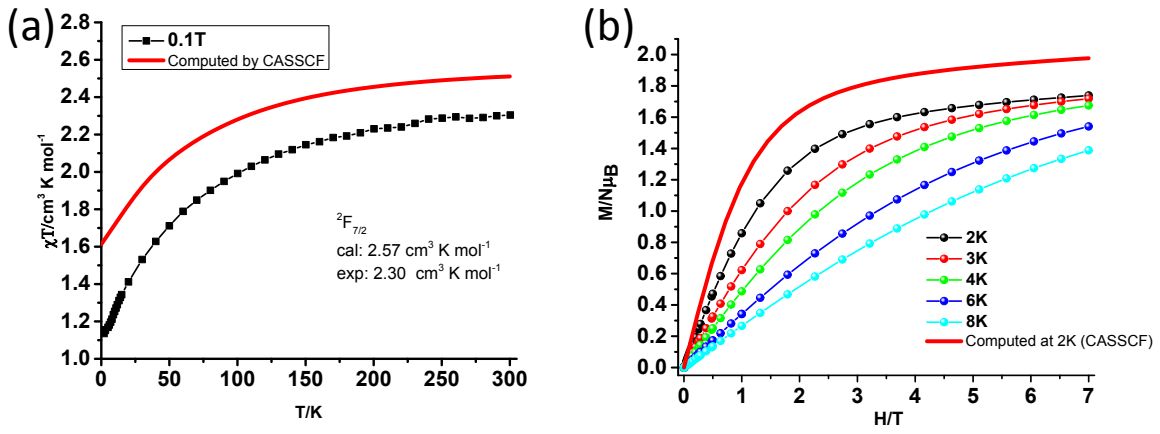

Figure S21: (a) Comparison of the computed magnetic susceptibility of **1** with experiment. Black spheres correspond to the experimental magnetic susceptibility data for **1**. (b) Comparison of computed molar magnetisation of **1** with experiment. The solid red line corresponds to the *ab initio* computed value.

Table-S13. The *ab initio* computed crystal field parameter of complex **1**, **2** and **3I$_2$**.

k	q	B_k^q (1)	B_k^q (2)	B_k^q (3I$_2$)	B_k^q (3a)
2	-2	9.80E-01	3.51E-01	4.35E-01	7.08E-01
	-1	1.71E-01	-8.97E-01	8.31E-01	7.05E-02
	0	**-5.23E+00**	**-8.90E+00**	**-1.67E+01**	**-5.35E+01**
	1	-1.51E+00	-3.57E+00	2.18E-01	-8.88E-02
	2	-2.92E+00	3.25E+00	-4.92E-01	-4.38E-02
4	-4	-4.96E-01	3.61E-01	-9.95E-01	-1.45E+00
	-3	-6.97E-02	1.71E-02	5.74E-02	2.90E-02
	-2	2.49E-02	-5.02E-02	1.21E-02	1.56E-02
	-1	-8.42E-03	5.14E-02	-3.39E-02	2.02E-03
	0	**-3.62E-02**	**-2.21E-01**	**-1.46E-01**	**-1.02E-01**
	1	4.40E-02	1.11E-01	-1.87E-02	3.45E-03
	2	-5.46E-02	-1.28E-02	-7.52E-03	-2.90E-03
	3	1.35E-01	2.14E-02	-3.56E-02	-4.25E-02
	4	7.10E-01	-1.17E+00	7.64E-01	-1.26E-02
6	-6	-2.86E-03	-1.17E-03	7.32E-04	1.04E-04
	-5	5.26E-03	4.51E-04	2.45E-03	1.32E-03
	-4	-5.84E-04	9.32E-03	-2.23E-02	-2.90E-02
	-3	-2.24E-03	8.70E-04	1.74E-03	6.05E-04
	-2	1.10E-03	1.53E-04	6.51E-04	9.85E-04
	-1	-3.01E-03	-3.48E-03	2.93E-04	-4.77E-04
	0	**-2.95E-03**	**9.73E-04**	**-1.01E-03**	**-2.23E-03**
	1	1.74E-02	-5.22E-03	-3.31E-04	-1.96E-04
	2	-1.40E-03	2.38E-03	-4.18E-04	-1.21E-04
	3	4.64E-03	5.76E-04	-6.66E-04	1.03E-04
	4	3.40E-03	-2.67E-02	1.72E-02	-9.14E-04
	5	-8.85E-03	3.53E-03	3.42E-03	3.03E-03
	6	1.75E-03	1.10E-03	8.92E-05	-6.87E-04

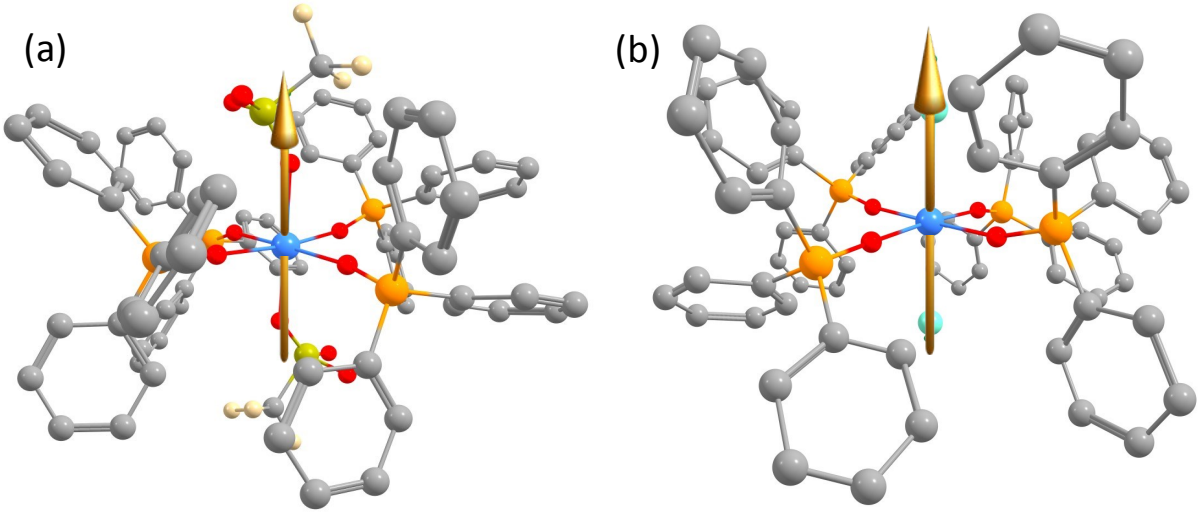

Figure S22: (a) The g_{zz} anisotropy axis of complex **2**. (b) The g_{zz} anisotropy axis of **3I$_2$**. Colour code: Yb-sky blue; I-cyan; O-red; N-blue; P-orange; S-green yellow; F-light yellow; C-grey. Hydrogens are omitted for clarity.

Table-S14. The energy of the four Kramers doublets along with g tensor of complex **2**.

Energy (cm^{-1})	***g_x***	***g_y***	***g_z***
0.0	0.188	0.890	6.882
329.3	0.329	1.665	5.516
392.1	0.337	1.905	5.660
567.1	4.368	3.576	1.251

Table-S15. The energy of the four Kramers doublets along with g tensor of **3I$_2$**.

Energy (cm^{-1})	***g_x***	***g_y***	***g_z***
0.0	0.129	0.172	7.663
447.5	3.630	3.541	3.025
663.4	5.056	3.688	0.793
691.9	4.346	2.878	0.715

Table-S16. The CAS(13,7) computed energy of the four Kramers doublets along with g tensor of **3IBr**.

Energy (cm^{-1})	***g_x***	***g_y***	***g_z***
0.0	0.136	0.201	7.627
430.7	3.694	3.608	2.848
627.5	4.597	4.173	0.791
665.9	3.881	3.452	0.578

Table-S17. The CAS(13,7) computed energy of the four Kramers doublets along with g tensor of **3ICl**.

Energy (cm^{-1})	***g_x***	***g_y***	***g_z***
0.0	0.229	0.34	7.392
350.3	3.948	3.855	1.795
470.4	4.629	3.901	0.552
566.2	4.223	3.602	0.463

Table-S18. The CAS(13,7) computed energy of the four Kramers doublets along with g tensor of **3BrCl**.

Energy (cm^{-1})	***g_x***	***g_y***	***g_z***
0.0	0.287	0.416	7.260
339.0	3.995	3.882	1.486
444.9	4.388	3.972	0.395
550.1	4.079	3.821	0.771

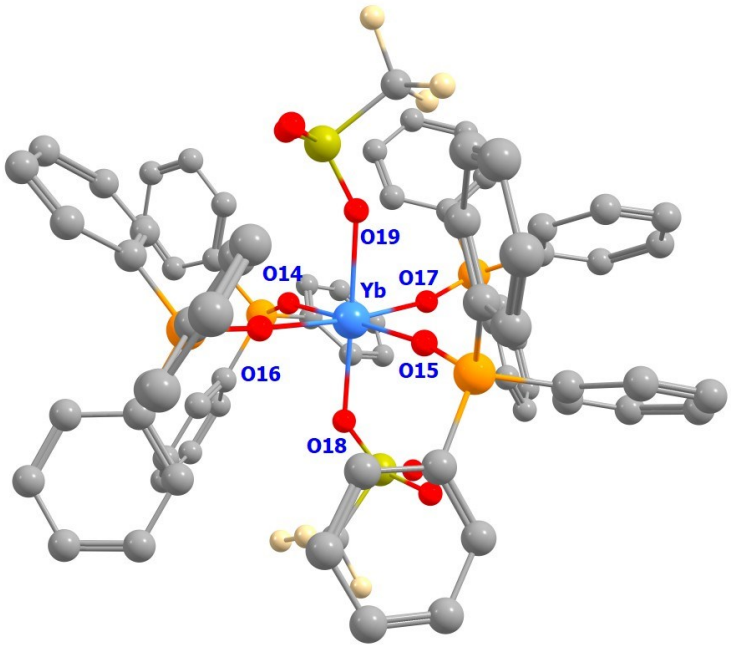

Figure S23: Model for Atom number with LoProp charge of **2**. Colour code: Yb-sky blue; O-red; N-blue; P-orange; S-green yellow; F-light yellow; C-grey. Hydrogens are omitted for clarity.

Table-S19. LoProp charge of Yb and coordinated atoms with Yb of complex **2**.

Atom	LoProp charge
Yb	2.5818
O18	-0.9981
O19	-1.0493
O14	-1.0914
O15	-1.1025
O16	-1.0960
O17	-1.0936

Table-S20. The comparison of LoProp charge of the Yb and axial atoms in **3I_2**, **3IBr**, **3ICl** and **3BrCl**.

Atom	3I_2	Atom	3IBr	Atom	3ICl	Atom	3BrCl
Yb	2.4246	Yb	2.4466	Yb	2.4629	Yb	2.4837
I2	-0.8202	I	-0.8144	I	-0.8276	Br	-0.8555
I3	-0.8148	Br	-0.8498	Cl	-0.8623	Cl	-0.8622
O8	-1.0935	O8	-1.0936	O8	-1.0894	O8	-1.0893
O9	-1.0880	O9	-1.0878	O9	-1.0831	O9	-1.0829
O10	-1.0854	O10	-1.0856	O10	-1.0809	O10	-1.0810
O11	-1.0898	O11	-1.0902	O11	-1.0846	O11	-1.0849

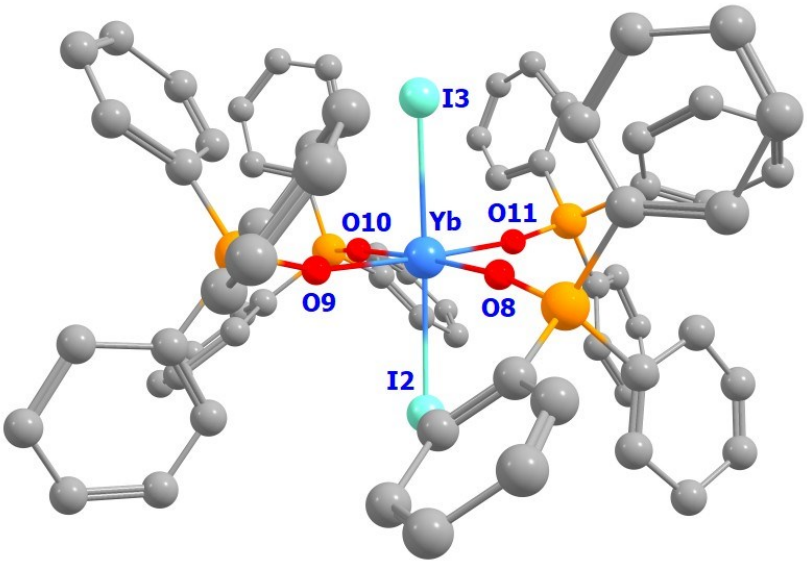

Figure S24: Model for Atom number with LoProp charge of **3** (**3I$_2$**). Colour code: Yb-sky blue; O-red; N-blue; P-orange; S-green yellow; F-light yellow; C-grey. Hydrogens are omitted for clarity.

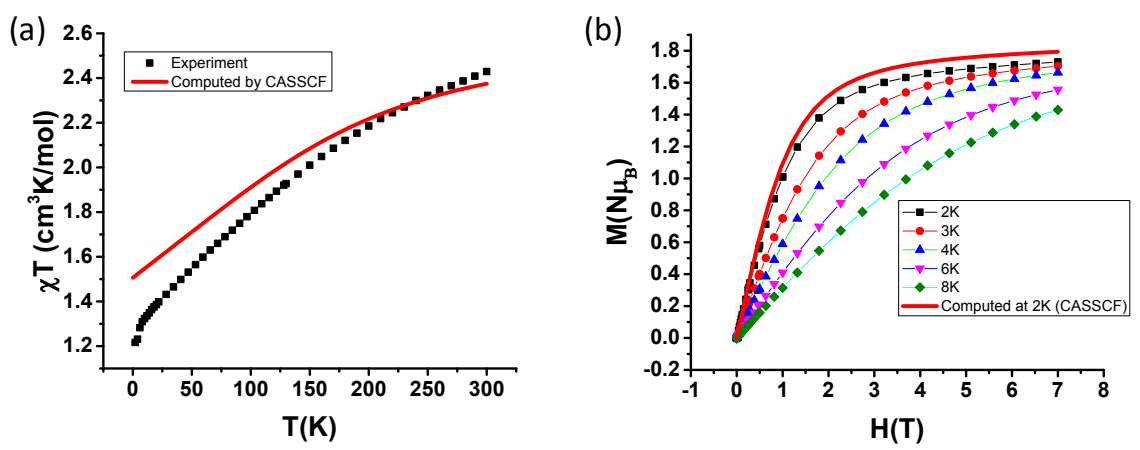

Figure S25: (a) Comparison of the computed magnetic susceptibility of **2** with experiment. Black spheres correspond to the experimental magnetic susceptibility data for **2**. The solid red line is the computed magnetic susceptibilities. (b) Comparison of computed molar magnetisation of **2** with experiment. The solid red line corresponds to the ab initio computed value.

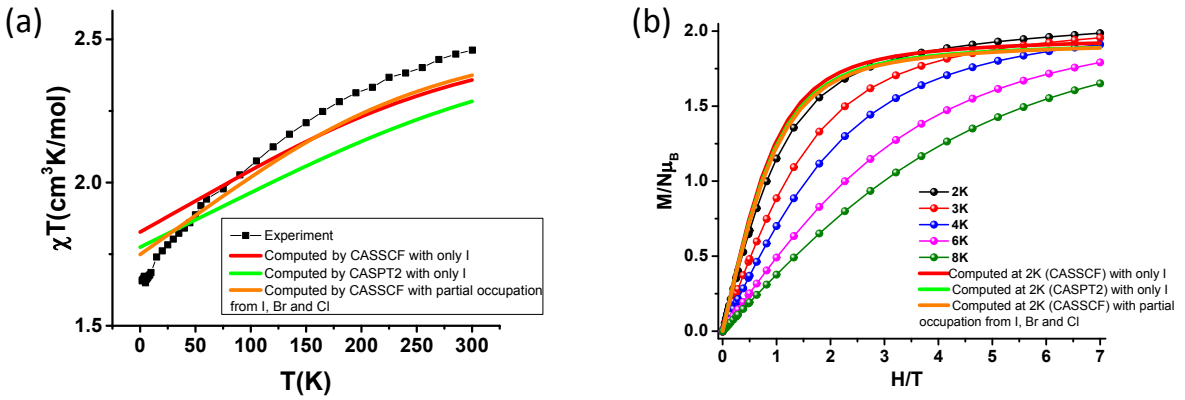

Figure S26: To understand the role of dynamic correlation on the magnetic anisotropy and the estimated barrier heights, further calculations were performed on model systems wherein the phenyl groups in complex **3** (**3I$_2$**) are replaced by methyl groups. The CASSCF calculation yield barrier height which is similar to the original complex while CASPT2 found to enhance the U_{eff} further worsening the match (also the estimated susceptibility, see Table S22-23). As dynamic correlation reveals deviation in the estimated barrier, incorporation of ligand atoms in the active space may improve the estimated barrier height, but these calculations are only a distant possibility at present, even for yet unknown models. (a) Comparison of the computed magnetic susceptibility of **3** with experiment. Black spheres correspond to the experimental magnetic susceptibility data for **3**. (b) Comparison of computed molar magnetisation of **3** with experiment. The solid red line corresponds to the computed value with CAS (13,7) on **3I$_2$** (only iodide in both axial position). The solid green line corresponds to the computed value with CASPT2 on **3I$_2$**. The solid orange line corresponds to the weightage computed value of **3** from partial occupation of I, Br and Cl in the axial position.

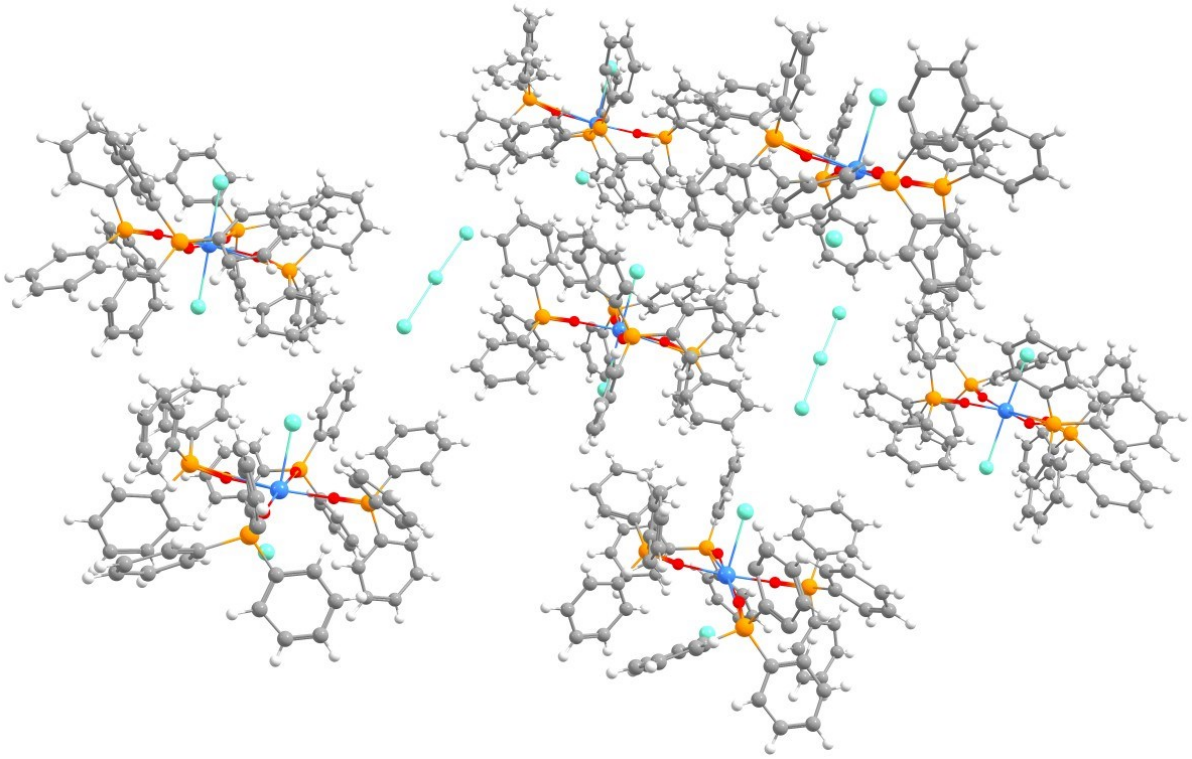

Figure S27: Supercell model of **3I$_2$**. Colour code: Yb-sky blue; O-red; N-blue; P-orange; S-green yellow; F-light yellow; C-grey. Hydrogens are omitted for clarity. "To estimate the lattice effect on the barrier heights, additional calculations were performed using the point charge model on **3I$_2$** wherein neighbouring molecules in the crystal lattice were replaced by point charges. The calculations yield only marginal alteration to estimate the barrier height and ligand field parameters (see Table S21 for lattice effects)."

Table-S21. The energy of the four Kramers doublets along with g tensor of the supercell of complex **3I$_2$**.

Energy (cm^{-1})	***g_x***	***g_y***	***g_z***
0.0	0.056	0.221	7.688
465.3	3.222	3.301	3.688
690.9	0.796	2.233	5.943
717.6	0.753	1.401	5.334

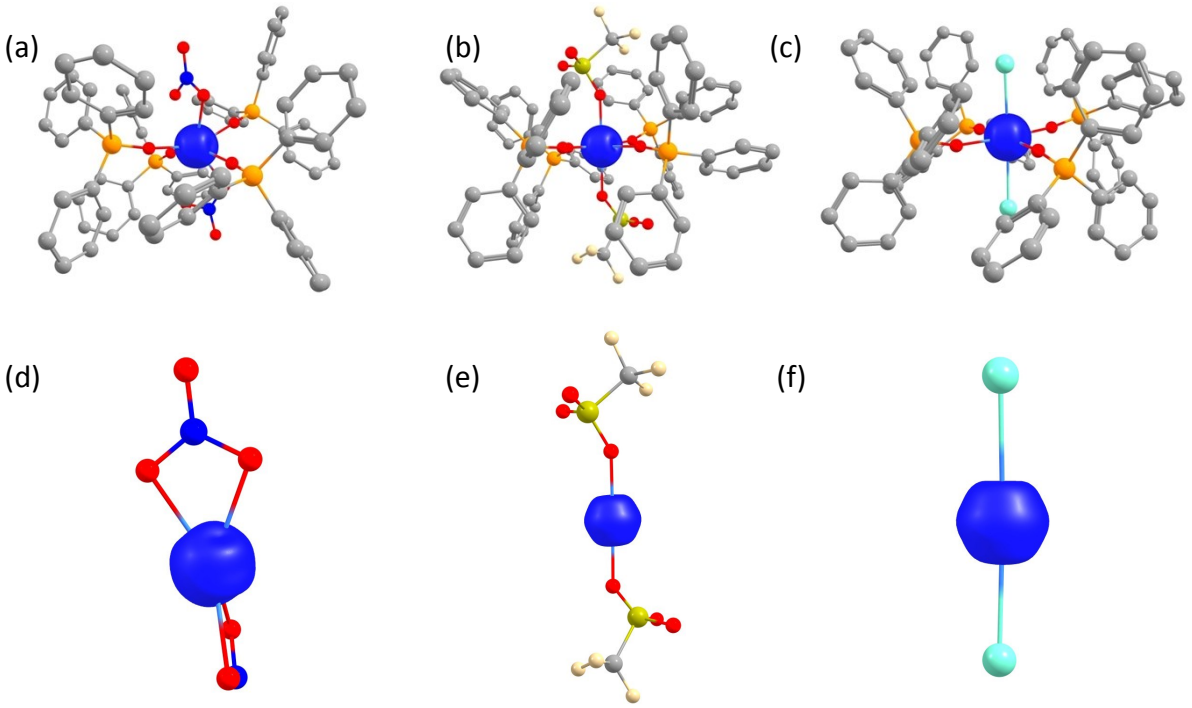

Figure S28: The beta electron density of Yb (III) in **1** (a) **2** (b) **3** (**3I$_2$**) (c) **1b** (d) **2b** (e) and **3b** (**3I$_2$**) (f). Colour code: Yb-sky blue; O-red; N-blue; P-orange; S-green yellow; F-light yellow; C-grey. Hydrogens are omitted for clarity.

Table-S22. The CAS(13,7) computed energy of the four Kramers doublets along with g tensor of the modelled complex of **3** (**3I$_2$**).

Energy (cm^{-1})	***g_x***	***g_y***	***g_z***
0.0	0.152	0.225	7.589
415.7	3.743	3.670	2.694
599.4	5.436	3.260	0.715
656.0	4.828	2.647	0.393

Table-S23. The CASPT2 computed energy of the four Kramers doublets along with g tensor of the modelled complex of **3** (**3I$_2$**).

Energy (cm^{-1})	***g_x***	***g_y***	***g_z***
0.0	0.192	0.246	7.527
533.4	3.916	3.841	1.963
660.1	5.123	3.512	0.657
835.0	4.631	3.170	0.315

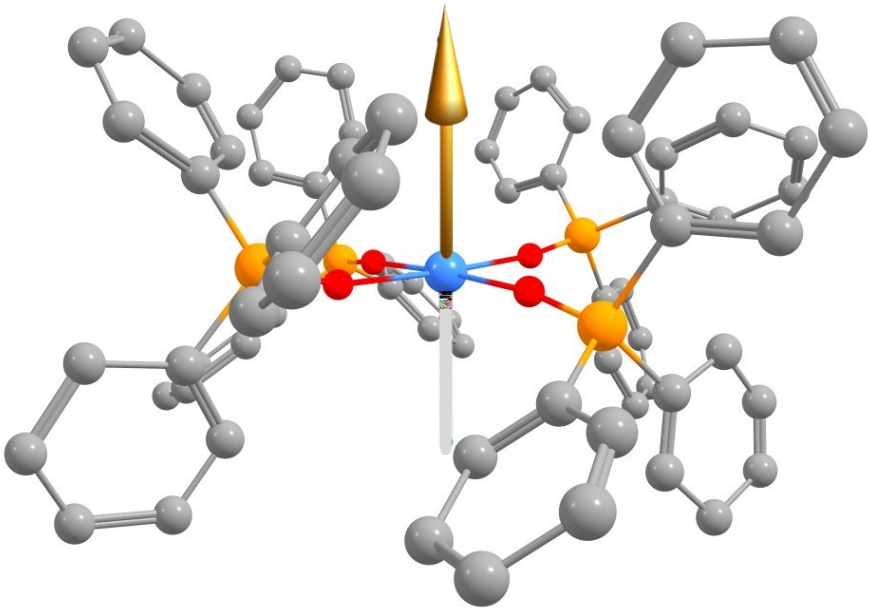

Figure S29: The g_{zz} anisotropy axis of complex **3a** (**3I$_2$**). Colour code: Yb-sky blue; O-red; N-blue; P-orange; S-green yellow; F-light yellow; C-grey. Hydrogens are omitted for clarity.

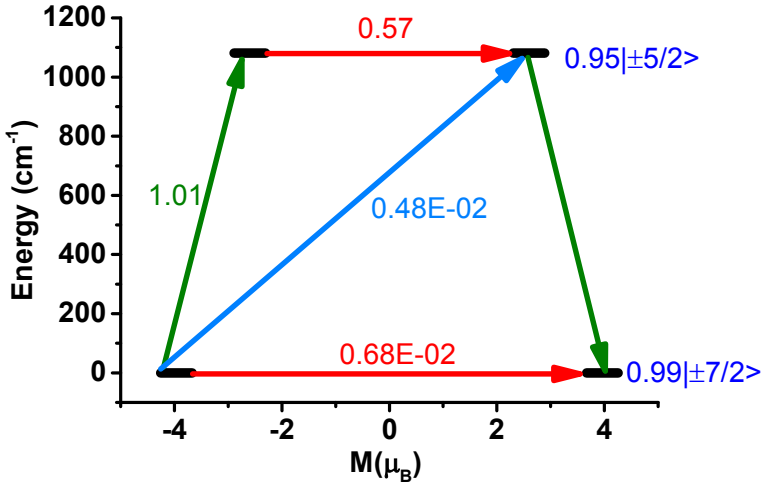

Figure S30: Mechanism of magnetic relaxation of complex **3a** (**3I$_2$**). The red line indicates the QTM and TA-QTM via ground KD and excited KD respectively. The olive line indicates the transition probability between KD1 and KD2. The sky-blue line indicates mechanism of orbach relaxation. The blue characters indicate the m_J composition of each KD.

Table-S24. The energy of the four Kramers doublets along with *g* tensor of **3a** (**3I$_2$**).

Energy (cm^{-1})	g_x	g_y	g_z
0.0	0.010	0.031	7.924
1081.0	1.700	1.713	5.190
1681.6	1.562	1.878	2.940
1984.4	4.691	4.374	1.074

Table-S25. The energy of the four Kramers doublets along with g tensor of complex **1b**.

Energy (cm^{-1})	g_x	g_y	g_z
0.0	5.307	3.760	1.101
154.5	0.668	0.878	3.432
702.2	0.066	0.085	5.747
1432.2	0.009	0.009	8.001

Table-S26. The energy of the four Kramers doublets along with g tensor of complex **2b**.

Energy (cm^{-1})	g_x	g_y	g_z
0.0	5.123	4.009	1.173
516.5	0.548	0.560	3.472
1187.9	0.002	0.016	5.756
2015.0	0.006	0.006	8.002

Table-S27. The energy of the four Kramers doublets along with g tensor of complex **3b** (**3I$_2$**).

Energy (cm^{-1})	g_x	g_y	g_z
0.0	4.595	4.551	1.166
269.6	0.011	0.031	3.469
741.3	0.006	0.015	5.749
1394.4	0.005	0.004	8.002

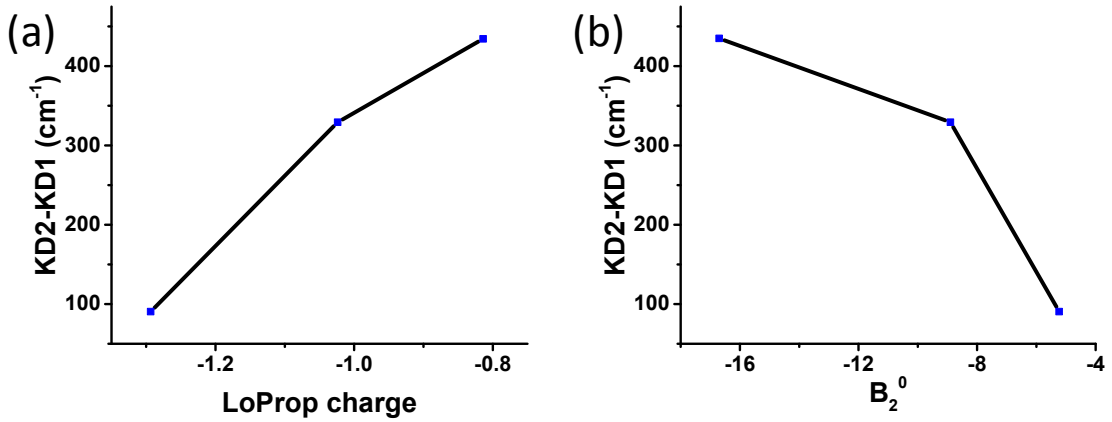

Figure S31: (a) The energy of the KD2-KD1 with average LoProp charge of axial atoms coordinated to metal. (b) The energy of the KD2-KD1 with the B_2^0 axial crystal field parameter.

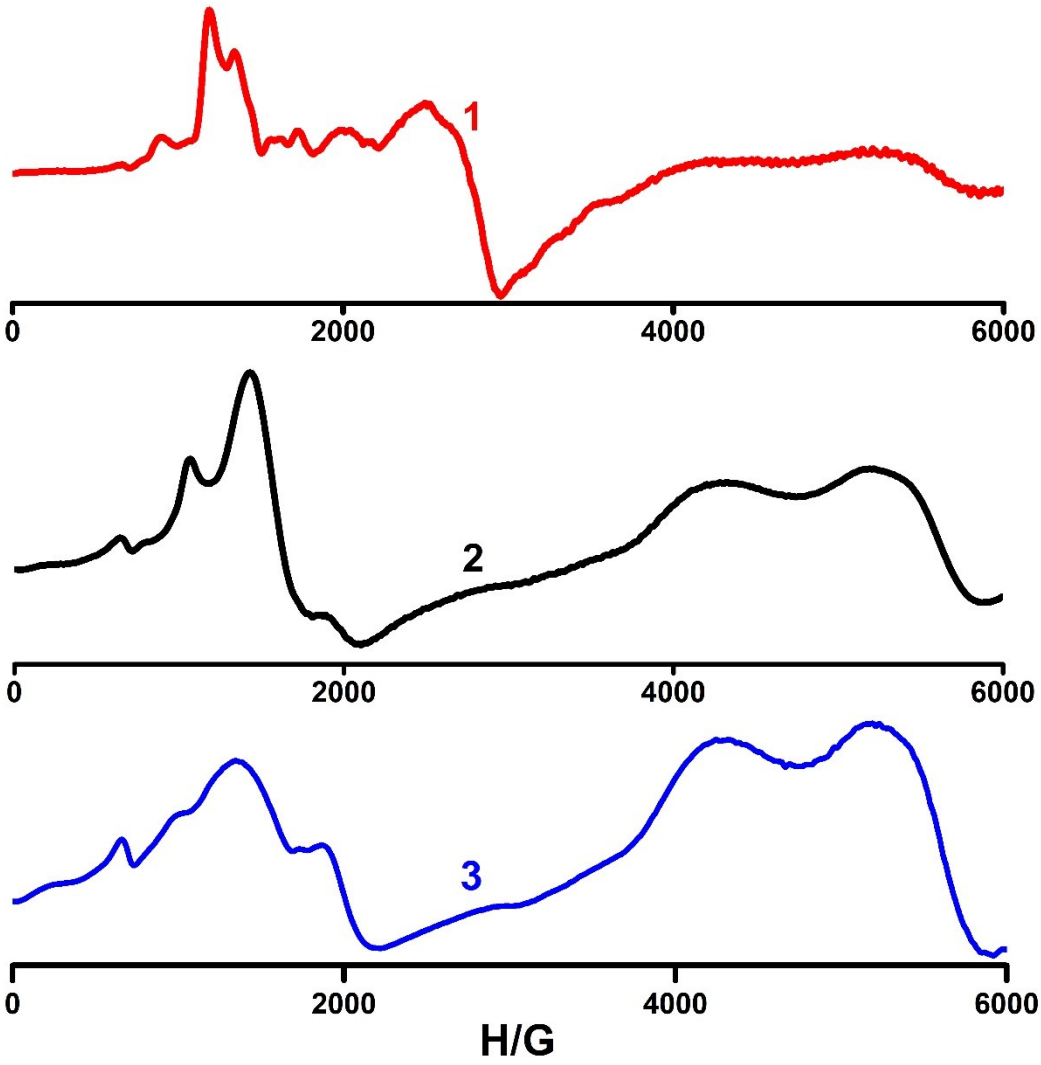

Figure S32: Solid state X-band EPR spectra of **1, 2** and **3** at 5 K.

SAIF/IIT BOMBAY

Operator ID:	IIT-B
Company name:	ThermoFinnigan
Method filename:	C:\2015-2016\13-02-2020-CHNS.mth
Method name:	Nitrogen/Carbon/Hydrogen/Sulphur
Analysed:	02/13/2020 22:10
Printed:	02-14-2020 14:48
Elemental Analyser method:	
Sampler method:	
Sample ID:	13-02-2020CHNS-013-ADITYA-ADI-428-YB-D4H (# 13)
Analysis type:	UnkNown
Chromatogram filename:	13-02-2020CHNS-013-ADITYA-ADI-428-YB-D4H.dat
Calibration method:	K Factors
Sample weight:	2.272
Protein factor:	6.25

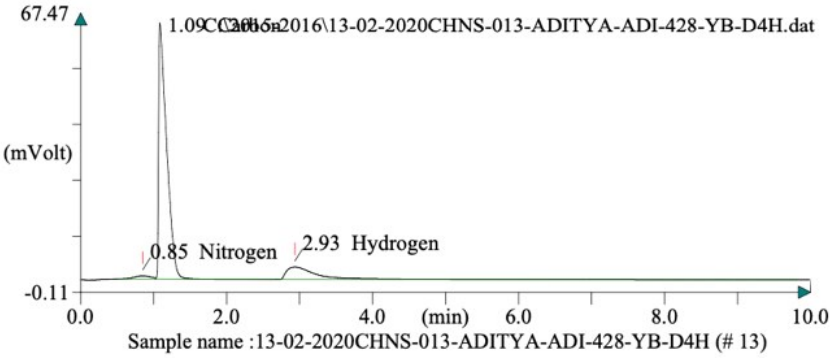

Peak Number (#)	Retention Time (min)	Area (.1*uV*sec)	Element %	Component N
1	0.850	118950	0.000	Nitrogen
2	1.092	4711617	45.494	Carbon
3	2.933	943831	3.234	Hydrogen
		5774398	48.729	

Figure S33a. Elemental analysis for the single crystals of **3**.

SAIF/IIT BOMBAY

Operator ID:	IIT-B
Company name:	ThermoFinnigan
Method filename:	C:\2015-2016\13-02-2020-CHNS.mth
Method name:	Nitrogen/Carbon/Hydrogen/Sulphur
Analysed:	02/13/2020 22:21
Printed:	02-14-2020 14:48
Elemental Analyser method:	
Sampler method:	
Sample ID:	13-02-2020CHNS-014-ADITYA-YB-D4H (# 14)
Analysis type:	UnkNown
Chromatogram filename:	13-02-2020CHNS-014-ADITYA-YB-D4H.dat
Calibration method:	K Factors
Sample weight:	2.326
Protein factor:	6.25

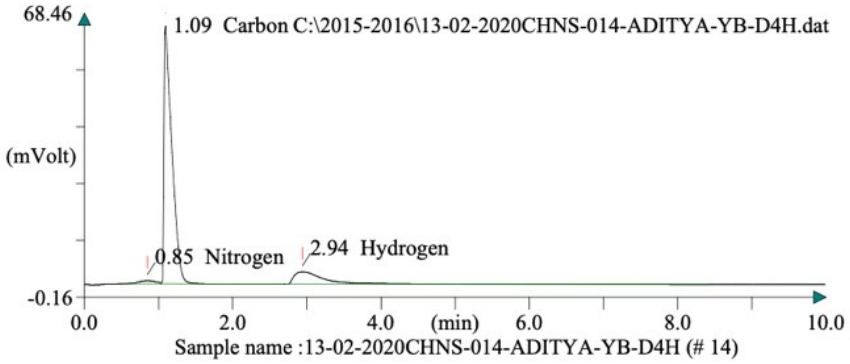

Sample name :13-02-2020CHNS-014-ADITYA-YB-D4H (# 14)

Peak Number (#)	Retention Time (min)	Area (.1*uV*sec)	Element %	Component N
1	0.850	119126	0.000	Nitrogen
2	1.092	4630150	43.670	Carbon
3	2.942	943994	3.160	Hydrogen
		5693270	46.830	

Figure S33b. Elemental analysis for the polycrystalline sample of **3** (batch A).

SAIF/IIT BOMBAY

Operator ID:	IIT-B
Company name:	ThermoFinnigan
Method filename:	C:\2015-2016\13-02-2020-CHNS.mth
Method name:	Nitrogen/Carbon/Hydrogen/Sulphur
Analysed:	02/13/2020 22:31
Printed:	02-14-2020 14:49
Elemental Analyser method:	
Sampler method:	
Sample ID:	13-02-2020CHNS-015-ADITYA-ADI-E-I (# 15)
Analysis type:	UnkNown
Chromatogram filename:	13-02-2020CHNS-015-ADITYA-ADI-E-I.dat
Calibration method:	K Factors
Sample weight:	2.44
Protein factor:	6.25

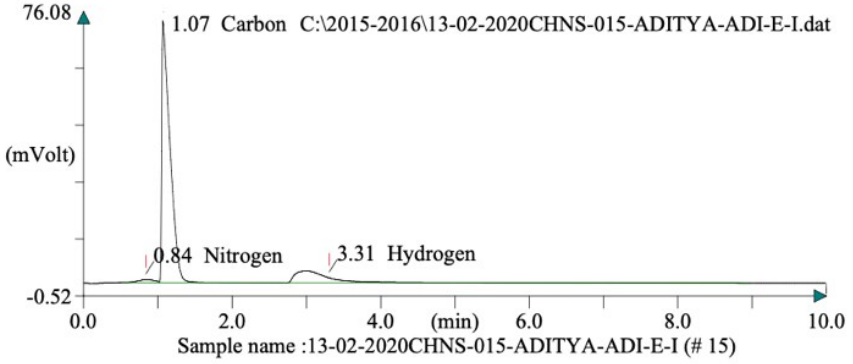

Sample name :13-02-2020CHNS-015-ADITYA-ADI-E-I (# 15)

Peak Number (#)	Retention Time (min)	Area (.1*uV*sec)	Element %	Component N
1	0.842	117366	0.000	Nitrogen
2	1.075	5379898	48.370	Carbon
3	3.308	1164408	3.741	Hydrogen
		6661672	52.111	

Figure S33c. Elemental analysis for the polycrystalline sample of **3** (batch B)

References :

1. W. L. F. Armarego, *Purification of laboratory chemicals*, Butterworth-Heinemann, 2017.
2. O. V. Dolomanov, L. J. Bourhis, R. J. Gildea, J. A. Howard and H. Puschmann, *J. Appl. Cryst.*, 2009, **42**, 339-341.
3. G. M. Sheldrick, *Acta Crystallogr., Sect. A: Found. Adv*, 2015, **71**, 3-8.
4. G. M. Sheldrick, *Acta Crystallogr. C*, 2015, **71**, 3-8.
5. M. Llunell, D. Casanova, J. Cirera, P. Alemany and S. Alvarez, *University of Barcelona, Barcelona*, 2010.
6. J.-L. Liu, K. Yuan, J.-D. Leng, L. Ungur, W. Wernsdorfer, F.-S. Guo, L. F. Chibotaru and M.-L. Tong, *Inorg. Chem.*, 2012, **51**, 8538-8544.
7. D.-Q. Wu, D. Shao, X.-Q. Wei, F.-X. Shen, L. Shi, Y.-Q. Zhang and X.-Y. Wang, *Dalton Trans.*, 2017, **46**, 12884-12892.
8. K. S. Pedersen, J. Dreiser, H. Weihe, R. Sibille, H. V. Johannesen, M. A. Sørensen, B. E. Nielsen, M. Sigrist, H. Mutka and S. Rols, *Inorg. Chem.*, 2015, **54**, 7600-7606.
9. W. Zhao, H. Cui, X.-Y. Chen, G. Yi, L. Chen, A. Yuan and C.-L. Luo, *Dalton Trans.*, 2019, **48**, 5621-5626.
10. K. Soussi, J. Jung, F. Pointillart, B. Le Guennic, B. Lefeuvre, S. Golhen, O. Cador, Y. Guyot, O. Maury and L. Ouahab, *Inorg. Chem. Front.*, 2015, **2**, 1105-1117.
11. W. Huang, J. Xu, D. Wu, X. Huang and J. Jiang, *New J. Chem.*, 2015, **39**, 8650-8657.
12. A. A. Trifonov, B. Shestakov, J. r. m. Long, K. Lyssenko, Y. Guari and J. Larionova, *Inorg. Chem.*, 2015, **54**, 7667-7669.
13. Q. Zou, X.-D. Huang, J.-C. Liu, S.-S. Bao and L.-M. Zheng, *Dalton Trans.*, 2019, **48**, 2735-2740.
14. M. E. Boulon, G. Cucinotta, J. Luzon, C. Degl'Innocenti, M. Perfetti, K. Bernot, G. Calvez, A. Caneschi and R. Sessoli, *Angew. Chem. Int. Ed.*, 2013, **52**, 350-354.
15. A. Lannes and D. Luneau, *Inorg. Chem.*, 2015, **54**, 6736-6743.
16. F. Aquilante, J. Autschbach, R. K. Carlson, L. F. Chibotaru, M. G. Delcey, L. De Vico, I. Fdez. Galván, N. Ferré, L. M. Frutos and L. Gagliardi, *J. Comput. Chem.*, 2016, **37**, 506-541.
17. M. Reiher, *Wiley Interdiscip. Rev. Comput. Mol. Sci*, 2012, **2**, 139-149.
18. A. Wolf, M. Reiher and B. A. Hess, *J. Chem. Phys.*, 2002, **117**, 9215-9226.
19. L. F. Chibotaru, L. Ungur and A. Soncini, *Angew. Chem. Int. Ed.*, 2008, **47**, 4126-4129.
20. L. F. Chibotaru and L. Ungur, *J. Chem. Phys.*, 2012, **137**, 064112.